

Statistical Comparison of Spike Responses to Natural Stimuli in Monkey Area V1 With Simulated Responses of a Detailed Laminar Network Model for a Patch of V1

Malte J. Rasch, Klaus Schuch, Nikos K. Logothetis and Wolfgang Maass

J Neurophysiol 105:757-778, 2011. First published 24 November 2010; doi:10.1152/jn.00845.2009

You might find this additional info useful...

This article cites 103 articles, 49 of which can be accessed free at:

<http://jn.physiology.org/content/105/2/757.full.html#ref-list-1>

Updated information and services including high resolution figures, can be found at:

<http://jn.physiology.org/content/105/2/757.full.html>

Additional material and information about *Journal of Neurophysiology* can be found at:

<http://www.the-aps.org/publications/jn>

This information is current as of March 23, 2011.

Statistical Comparison of Spike Responses to Natural Stimuli in Monkey Area V1 With Simulated Responses of a Detailed Laminar Network Model for a Patch of V1

Malte J. Rasch,^{1,2,3*} Klaus Schuch,^{1*} Nikos K. Logothetis,^{3,4} and Wolfgang Maass¹

¹Institute for Theoretical Computer Science, Graz University of Technology, Graz, Austria; ²Institute of Neuroscience, Chinese Academy of Science, Shanghai, China; ³Max Planck Institute for Biological Cybernetics, Tübingen, Germany; and ⁴Imaging Science and Biomedical Engineering, University of Manchester, Manchester, United Kingdom

Submitted 15 September 2009; accepted in final form 21 November 2010

Rasch MJ, Schuch K, Logothetis NK, Maass W. Statistical comparison of spike responses to natural stimuli in monkey area V1 with simulated responses of a detailed laminar network model for a patch of V1. *J Neurophysiol* 105: 757–778, 2011. First published November 24, 2010; doi:10.1152/jn.00845.2009. A major goal of computational neuroscience is the creation of computer models for cortical areas whose response to sensory stimuli resembles that of cortical areas in vivo in important aspects. It is seldom considered whether the simulated spiking activity is realistic (in a statistical sense) in response to natural stimuli. Because certain statistical properties of spike responses were suggested to facilitate computations in the cortex, acquiring a realistic firing regimen in cortical network models might be a prerequisite for analyzing their computational functions. We present a characterization and comparison of the statistical response properties of the primary visual cortex (V1) in vivo and in silico in response to natural stimuli. We recorded from multiple electrodes in area V1 of 4 macaque monkeys and developed a large state-of-the-art network model for a 5 × 5-mm patch of V1 composed of 35,000 neurons and 3.9 million synapses that integrates previously published anatomical and physiological details. By quantitative comparison of the model response to the “statistical fingerprint” of responses in vivo, we find that our model for a patch of V1 responds to the same movie in a way which matches the statistical structure of the recorded data surprisingly well. The deviation between the firing regimen of the model and the in vivo data are on the same level as deviations among monkeys and sessions. This suggests that, despite strong simplifications and abstractions of cortical network models, they are nevertheless capable of generating realistic spiking activity. To reach a realistic firing state, it was not only necessary to include both N-methyl-D-aspartate and GABA_B synaptic conductances in our model, but also to markedly increase the strength of excitatory synapses onto inhibitory neurons (>2-fold) in comparison to literature values, hinting at the importance to carefully adjust the effect of inhibition for achieving realistic dynamics in current network models.

INTRODUCTION

Numerical simulations of detailed biophysical models of cortical microcircuits or even whole brain regions provide powerful tools to approach complex questions in neuroscience and are commonly regarded as a promising tool to understand the mechanistic link from anatomical structure and physiological properties to computational functions of cortical circuits. In general, approaches along this line incorporate selected

aspects of the known anatomy and physiology to replicate experimental data on emergent functional properties, such as the structure of preferred orientation maps of the primary visual cortex (Adorjan et al. 1999; Bartsch and van Hemmen 2001; Blumenfeld et al. 2006), direction selectivity maps (Ernst et al. 2001; Wensch et al. 2005), and simple/complex cells (Chance et al. 1999; Tao et al. 2004; Wielaard et al. 2001), or successfully exemplifying theoretical ideas about information processing in the brain (Diesmann et al. 1999; Maass et al. 2002; Vogels and Abott 2005). However, these increasingly complex recurrent network models are often still a strong abstraction from reality, and it is not clear whether the responses of such network models exhibit at least a general likeness to its counterpart in reality.

Constraining the firing regimen of in silico models with that observed in vivo is important for at least two reasons: First, it will benchmark current models to achieve a realistic firing response and thus will further help to open new research directions because it will hint at current shortcomings of existing models. Second, it has been suggested theoretically that there might be a firing regimen or state that is favorable for ongoing computation within recurrent neural networks (Brunel 2000; Legenstein and Maass 2007; Vogels and Abbott 2005). One might thus postulate that, during evolution, the brain has shaped a particular useful firing regimen that is in some way supporting the computational function of the neural tissue. Therefore achieving a realistic firing activity in cortical circuit models might be an important but rarely considered prerequisite to using these models for analyzing aspects of cortical computational functions. If a realistic firing regimen cannot be achieved easily, the validity of conclusions drawn from these model circuits might be corrupted, or efforts have to be made to tune these models toward a realistic regimen. To study this issue, we ask in this study whether a state-of-the-art network model of a cortical circuit is able to reproduce the characteristic firing regimen of the cortex.

We focus on the primary visual system (V1) in the anesthetized state, because the anatomical and neurophysiological details of V1 are relatively well known and its position in visual sensory processing is relatively well established. In contrast to awake and behaving monkeys, the visual input received by V1 during stimulation is easily constrained by the experimenter. Moreover, V1 already serves as a reference cortical area to study large-scale network models (Johansson and Lansner 2007; Kremkow et al. 2007), although many

* M. J. Rasch and K. Schuch contributed equally to this work.

Address for reprint requests and other correspondence: M. J. Rasch, Institute of Neuroscience, Chinese Academy of Science, Yue Yang Road 320, Shanghai, China. (E-mail: malte@ion.ac.cn).

aspects of its computational organization and the underlying mechanisms remain poorly understood (Olshausen and Field 2005).

To compare the firing state of V1 *in vivo* with that of simulated responses of a cortical network model *in silico*, we first recorded spike responses with multielectrode arrays in V1 of four anesthetized monkeys while presenting seminatural movies of several-minute duration. Given the complex naturalistic stimuli, we thus expect that V1 will likely be in an operating regimen, where its computations are usually performed. We characterized this firing regimen by its “statistical fingerprint” using a number of salient statistical features, measuring the spike variability, the burst behavior, and the correlation structure. We compared this “statistical fingerprint” to that obtained from the response of a state-of-the-art cortical circuit model of a 5×5 -mm patch of V1, comprising about 35,000 neurons and 3.9 million synapses situated in several hypercolumns. The developed spiking neuron network model is based on the cortical microcircuit model described in Hauesler and Maass (2007), which implements experimental data from Thomson et al. (2002) on lamina-specific connection probabilities and data from Markram et al. (1998) and Gupta et al. (2000) regarding stereotypical dynamic properties (such as paired pulse depression and paired pulse facilitation) of synaptic connections. We extended this cortical microcircuit model laterally and incorporated many anatomical properties of V1 in macaques to ensure the comparability to our *in vivo* recordings.

Our approach, using both electrophysiological recordings and model circuit simulation, provided us with the unique possibility to use the same movie stimuli for the model simulations and during *in vivo* recordings. Given this comparability, we were able to study whether the firing regimen of a model achieves a realistic state, and if not, whether a set of global parameters were sufficient to tune the models firing regimen to become more realistic.

We found that the response of the detailed model circuit adopts a firing regimen that is remarkably similar to the *in vivo* response and is on average close to the deviations across different sessions and different monkeys. This close match was achieved by tuning only a few parameters: an overall synaptic weight scaling factor compensating for the reduced number of modeled neurons, the relative synaptic weight from excitatory to inhibitory neurons, and the relative strength of patchy lateral long-range excitatory weights. We found that the firing response statistics was not simply induced by the statistics of the complex input stimuli but instead depended significantly on the internal dynamics. This good fit suggests that current network models comprising realistic neuron dynamics, as well as realistic time courses of synaptic activation, which included short-term depression and facilitation, are capable of generating a similar diverse network response behavior as can be observed in *in vivo* recordings.

Growing evidence suggests that computational functions of neural circuits are closely linked to its firing regimen. We therefore expect that this characterization of the firing regimen provided here and the possibility to use a few parameters to calibrate a complex model will greatly ease the analysis of the computational properties of realistic, detailed circuit models in future.

METHODS

Experimental methods

ELECTROPHYSIOLOGICAL RECORDING. The electrophysiological recordings were previously described in (Montemurro et al. 2008), where the same data were analyzed from a different perspective. However, for completeness we include a detailed description here.

Four adult rhesus monkeys (*Macaca mulatta*) participated in these experiments. All procedures were approved by the local authorities (Regierungspräsidium) and were in full compliance with the guidelines of the European Community (EUVD 86/609/EEC) for the care and use of laboratory animals. Before the experiments, form-fitted head posts and recording chambers were implanted during an aseptic and sterile surgical procedure (Logothetis et al. 2002). To perform the neurophysiological recordings, the animals were anesthetized (remifentanyl, 0.5–2 $\mu\text{g}/\text{kg}/\text{min}$), intubated, and ventilated. Muscle relaxation was achieved with a fast acting paralytic, mivacurium chloride (5 mg/kg/h). Body temperature was kept constant, and lactated Ringer solution was given at a rate of 10 ml/kg/h. During the entire experiment, the vital signs of the monkey and the depth of anesthesia were continuously monitored (as described in Logothetis et al. 1999). For the protocol used in these experiments, we previously examined the concentration of all stress hormones (catecholamines) (Logothetis et al. 1999) and found them to be within the normal limits. Drops of 1% ophthalmic solution of anticholinergic cyclopentolate hydrochloride were instilled into each eye to achieve cycloplegia and mydriasis. Refractive errors were measured, and contact lenses (hard PMMA lenses, Wöhlk) with the appropriate dioptric power were used to bring the animal's eye into focus on the stimulus plane. The electrophysiological recordings were performed with electrodes that were arranged in a 4×4 square matrix (interelectrode spacing varied from 1 to 2.5 mm) and introduced each experimental session into the cortex through the overlying dura mater by a microdrive array system (Thomas Recording, Giessen, Germany). Electrode tips were typically (but not always) positioned in the upper or middle cortical layers. The impedance of the electrode varied from 300 to 800 kOhm. Both spontaneous and stimulus-induced neural activity were collected and recorded for periods ≤ 6 min. Signals were amplified using an Alpha Omega amplifier system (Alpha Omega, Ubstadt-Weiher, Germany). The amplifying system filtered out the frequencies below 1 Hz. Recordings were performed in a darkened booth (Illtec, Illbruck Acoustic). The receptive fields of the electrode sites were plotted manually, and the position and size of each field were stored together with the stimulus parameters and the acquisition data. The visual stimulator was a dual processor Pentium II workstation running Windows NT (Intergraph, Huntsville, AL) and equipped with OpenGL graphics cards (3Dlabs Wildcat series). The resolution was set to 640 by 480 pixels. The refresh rate was 60 Hz, and the movie frame rate was 30 Hz. All image generation was in 24-bit true-color, using hardware double buffering to provide smooth animation. The 640×480 VGA output drove the video interface of a fiber-optic stimulus presentation system (Avotec, Silent Vision) and also drove the experimenter's monitor. The field of view (FOV) of the system was $30 \text{ H} \times 23 \text{ V}$ degrees of visual angle and the focus was fixed at 2 diopters. The system's effective resolution, determined by the fiber-optic projection system was $800 \text{ H} \times 225 \text{ V}$ pixels (the fiber-optic bundle is 530×400 fibers). Binocular presentations were accomplished through two independently positioned plastic, fiber-optic glasses. Positioning was aided by a modified fundus camera (Zeiss RC250) that permitted simultaneous observation of the eye fundus. The fundus camera has a holder for avotec projector so that the center of camera lens and avotec projector is aligned in the same axis. This process ensured the alignment of the stimulus center with the fovea of each eye. To ensure accurate control of stimulus presentation, a photo-diode was attached to the experimenter's monitor

permitting the recording of the exact presentation time of every single frame.

The visual stimuli were binocularly presented 3.5- to 6-min-long natural color movies (segments of the commercial movie "Star Wars"). During each of 10 recording sessions, the movie was repeated 12–40 times.

SPIKE DETECTION. To extract spike times from the electrophysiological recordings, the 20.83 kHz neural signal was filtered in the high-frequency range of 500–3,500 Hz. The threshold for spike detection was set to 3.5 SD. A spike was recognized as such only if previous spikes have occurred >1 ms earlier. Spikes detected represent the spiking activity of a small population of cells rather than well-separated spikes from a single neuron. To separate this multiunit activity into single unit activity, we sorted the spikes according to the wave forms.

For spike sorting, we used the method described by Quian Quiroga et al. (2004). The spike waveforms were extracted around the detection times as described above (in a region of 0.25 ms before to 0.5 ms after the detected spike). These spike forms were interpolated, and 10 wavelet features (with 4 scales) were extracted (Quian Quiroga et al. 2004). From this feature pool, the 10 features (KS-test) were used as input for the clustering algorithm. We sorted the spikes using the paramagnetic algorithm of Quian Quiroga et al. (2004). For each electrode, a few reasonable clusters were selected by visual inspection of the spike waveforms ensuring a reasonable distinguishable average waveform among clusters. After this initial selection, spikes that initially were not classified in a particular cluster (or belonging to not selected clusters) were forced to belong to the nearest selected cluster (Mahalanobis distance; Quian Quiroga et al. 2004). A cluster that maintained very similar waveforms after this step was deemed to be a well-isolated cluster and was considered for further analysis. Otherwise the cluster was not considered further for spike sorting.

Model

In this section, we describe a data-based model developed to compare its spiking activity with the electrophysiological recordings from macaque. It consists of an input model [representing the retina and lateral geniculate nucleus (LGN) of the thalamus] and a model of a patch of V1, receiving and processing the spikes of the input model. In the following, we will first describe the V1 model and subsequently the input model.

V1 MODEL. Our model for a 5×5 -mm patch of area V1 consisted of 34,596 neurons and 3.9 million synapses. Various anatomical and physiological details were included in our model. The connectivity structure of the V1 model was similar to that of the generic cortical microcircuit model discussed in Haeusler and Maass (2007). The neurons of that model were equally distributed on three layers, corresponding to the cortical layers 2/3, 4, and 5. Each layer contained a population of excitatory neurons and a population of inhibitory neurons with a ratio of 4:1 (Beaulieu et al. 1992; Markram et al. 2004). The inter- and intralayer connectivity (probability and strength) was chosen according to experimental data from rat and cat cortex assembled in Thomson et al. (2002). Although there are differences, the connectivity structure in macaque is similar to that of the cat, in particular, if one identifies layer 2/3 and 4 in cat with 2-4B and 4C in macaque, respectively (Callaway 1998). The major geniculate input reaches in both species first layer 4C. Layer 4C projects to layer 2-4B, which in turn projects further to layer 5 (and layer 6 via layer 5), where feedback connections are made to layers 2-4B (see Callaway 1998 for a review). Furthermore, the sublaminar organization, e.g., the structure built by cytochrome-oxidase blobs in layer 2/3 (Callaway 1998), was neglected for simplicity and for the lack of precise data. However, as described below, the V1 model contained in addition to the microcircuit model of Haeusler and Maass (2007) a realistic

thalamic input, a smooth orientation map, and patchy long-range connections in the superficial layer.

In contrast to Haeusler and Maass (2007), we set the relative amount of neurons per layer to 33%. This partitioning corresponds to experimental data from macaques (Beaulieu et al. 1992; O'Kusky and Colonnier 1982; Tyler et al. 1998), although we slightly adjusted the relative amount of neurons compared with the experimental values (where layer 4 has ~33% more neurons), compensating for the fact that our model neglects the magnocellular and koniocellular pathways in favor of the parvocellular pathway (Callaway 1998). The three layers of the model can be identified with layers 2-4B, 4C β , and 5–6 in macaque V1. To avoid confusion with the terminology of (Haeusler and Maass 2007), we will, nevertheless, call them layer 2/3, 4, and 5 in the following.

In macaque, each of these three layers contains ~50,000 neurons under a surface area of 1 mm² (Beaulieu et al. 1992). In our model, we neglected that neuron density varies ≤ 1.5 -fold between the layers (Beaulieu et al. 1992) and assumed instead that the neurons are uniformly distributed throughout the cortex. Thus for simplicity, we positioned all neurons on a cuboid grid with constant grid spaces. Using the experimentally measured neuron density, e.g., for layer 2/3, the grid spacing would be 20 μ m for all directions. Because the simulation of such a dense network would take too much computation time, we diluted the neuron density by increasing the lateral grid spacing to 80 μ m and the vertical spacing to about 200 μ m.

We used a conductance-based single-compartment neuron model. Because of a considerable gain in computational speed, we used a neuron model suggested by Izhikevich (2003), which can be adjusted to express different firing dynamics (Izhikevich 2006). We randomly drew the parameters for each neuron in the network according to the bounds provided by Izhikevich et al. (2004). On the basis of these parameter distributions, the excitatory pools consisted of regular spiking cells, intrinsically bursting cells, and chattering cells, with a bias toward regular spiking cells. The inhibitory pools consisted of fast spiking neurons and low-threshold spiking neurons.

In addition to the synaptic input from other neurons in the model, each neuron received as additional input synaptic background input, modeling the bombardment of each neuron with synaptic inputs from a large number of neurons that are not represented in our model. This synaptic background input causes a depolarization of the membrane potential and a lower membrane resistance, commonly referred to as the "high conductance state" (Destexhe et al. 2001). The conductances of the background input was modeled according to Destexhe et al. (2001) by Ornstein-Uhlenbeck processes with means $g_{exc} = 0.012 \mu$ S and $g_{inh} = 0.047 \mu$ S, variances $\sigma_{exc} = p_1 0.003 \mu$ S and $\sigma_{inh} = p_1 0.0066 \mu$ S, and time constants $\tau_{exc} = 2.7$ ms and $\tau_{inh} = 10.5$ ms, where the indices exc/inh refer to excitatory and inhibitory background conductances, respectively. During the parameter optimization, we scaled the variances of both processes. The scaling factor p_1 of both variances affects the amount of noise added to the conductance of a neuron.

Short-term synaptic dynamics was implemented according to Markram et al. (1998), with synaptic parameters chosen as in Maass et al. (2002) to fit data from microcircuits in rat somatosensory cortex (based on Gupta et al. 2000 and Markram et al. 1998). For further details, we refer to Haeusler and Maass (2007).

Lateral connectivity structure. The generic microcircuit model of Haeusler and Maass (2007) was based on data for a column of about 100 μ m diam with uniform connectivity per layer and neuron type. Here we extended the model laterally to several millimeters. Thus connection probabilities in our model depend on the lateral distance. For inter- and intracortical connections, we generally used a bell-shaped (Gaussian) probability distribution for determining the lateral extent. The SD of the Gaussian was set to 200 μ m for excitatory neurons (Blasdel et al. 1985; Buzas et al. 2006; Lund et al. 2003) and to 150 μ m for inhibitory neurons to incorporate the observed occurrence of extremely narrow inhibitory dendritic and axonal spreads (70

μm ; Lund et al. 2003). The arborization of excitatory neurons in layer 5 seems to be wider, more diffuse, and has a spread of $>500\ \mu\text{m}$ laterally from the soma (Blasdel et al. 1985). Thus for these connections, we set the SD to $300\ \mu\text{m}$. Note that the value for the SD is about one half the expected maximal extent of 95% of the arborizations.

To ensure consistency with the connectivity data of Thomson et al. (2002), we scaled the Gaussian profiles such that the peak probabilities correspond to their experimentally measured connection probabilities. Therefore their connectivity pattern was locally preserved.

According to Song et al. (2005), the number of bidirectional connections between excitatory neurons in layer 5 is four times higher than the expected number under the assumption that the conditional probabilities, whether an unidirectional connection exists or not, are the same. We incorporated this probability increase into our model.

Patchy lateral long-range connections. In cat and macaque, many pyramidal cells in layer 2/3 of the striate cortex (and also elsewhere in the cortex; Lund et al. 2003) have characteristic long-range projections targeting laterally 80% excitatory and 20% inhibitory cells (McGuire et al. 1991), which are $\leq 6\ \text{mm}$ and more away (Buzas et al. 2006; Gilbert et al. 1996; Lund et al. 2003). Moreover, the targeted neurons tend to have similar feature preference as its origin, resulting in patchy connections linking similar preferred orientations (Buzas et al. 2006; Gilbert et al. 1996). Combining anatomical reconstructions of neurons and optical imaging of orientation maps, Buzas et al. (2006) proposed a formula to calculate the bouton density ρ of a typical layer 2/3 pyramidal cell

$$\rho(r, \Delta\varphi) = Z \left[\exp\left(-\frac{r^2}{2\sigma_1^2}\right) + m \exp\left(-\frac{r^2}{2\sigma_2^2}\right) \exp(\kappa \cos(2\Delta\varphi - 2\mu)) \right] \quad (1)$$

r is the lateral (Euclidean) distance between the pre- and the postsynaptic neuron, and $\Delta\varphi$ is the difference of preferred orientations of the two neurons. Parameter μ is an offset in the orientation preference and parameter m is a scaling factor that accounts for the importance of the long-range orientation-dependent term against the local orientation independent term. SD σ_1 and σ_2 regulate the spatial width of the nonoriented and oriented term, respectively. Parameter κ signifies the “peakiness” of the density on the orientation axis. Z is a normalization constant. Because we defined preferred orientations in a hard-wired manner via “oriented” input connections (see APPENDIX A), we applied Eq. 1 for the lateral connections in layer 2/3, more specifically, for projections from excitatory cells targeting excitatory and inhibitory cells (McGuire et al. 1991).

Analogous to connections between other layers, we set $\sigma_1 = 200\ \mu\text{m}$ for the local nonoriented term. We set $\mu = 0^\circ$ and $\sigma_2 = 1,000\ \mu\text{m}$ (estimated from the measurements of Buzas et al. 2006). We chose a higher $\kappa = 20$ than reported because of the following reasoning. As described above, the neuron density of our circuit model is much smaller than in reality. We compensated this neuron dilution by a noise process fed into each modeled neuron, which implicitly models activation of omitted neurons as described above (Destexhe et al. 2001). Because any (implicit) input from omitted neurons is independent of orientation preference, neurons in the circuit should have a strong bias toward orientation preference dependent connections. To account for this bias, we therefore increased κ .

Finally, the parameter m was set so that 58% of the excitatory synapses onto an excitatory neuron in layer 2/3 were long-range connections. As before, the connection probability was scaled, according to Thomson et al. (2002), by setting Z to appropriate values. Thus locally, i.e., for a neuron at the same lateral position (and orientation preference) such as a neuron located in the same layer beneath or above the presynaptic neuron, the connection probabilities were preserved. However, the weight distribution of the long-range connection was not constrained by Thomson et al. (2002). Hence, we simply scaled the recurrent weight reported by Thomson et al. (2002) and fitted the scaling factor to the in vivo data (see RESULTS). As standard value, we used a value of 1.0 for this parameter that is the same average weight as in Thomson et al. (2002).

Distance-dependent synaptic delay. Synaptic delays differ for inhibitory and excitatory neurons. They were set according to measurements by Gupta et al. (2000) (for details see Haeusler and Maass 2007). These delays stem from molecular processes of synaptic transmission. In addition, a second delay originating from finite spike propagation velocity of the fibers was included. This delay depends on the (Euclidean) distance between the pre- and the postsynaptic neuron. Girard et al. (2001) found a median conduction velocity of 0.3 m/s for the upper layers and 1 m/s for the lower layers of V1 in macaque monkeys. Thus we sampled the velocity for each excitatory synapse in layer 2/3 from a Gaussian distribution with mean 0.3 m/s and SD 0.5 m/s (with enforced lower and upper bounds of 0.05 and 5 m/s, respectively). For the other layers, the conduction velocities were drawn from a Gaussian distribution with mean 1 m/s and SD 0.9 m/s (with same bounds as before). Because of myelination, conduction velocities of inhibitory fibers are generally higher than for excitatory cells (Thomson et al. 2002). Lacking exact measurements in the literature for all inhibitory cells, we sampled the velocities from a distribution with mean and SD twice as high as for excitatory neurons in the deep layers (the enforced upper bound was set to 10 m/s).

Synaptic conductances. A spike, arriving at a synapse, causes a change in the synaptic conductance in the postsynaptic neuron. The dynamic of the conductance depends on the receptor kinetics. Each excitatory synapse in our model contains α -amino-3-hydroxy-5-methyl-4-isoxazolepropionic acid (AMPA) receptors having relatively fast kinetics (modeled as exponential decay with time constant $\tau_{\text{AMPA}} = 5\ \text{ms}$, reversal potential 0 mV). A fraction f_{NMDA} of all excitatory synapses contain additionally relatively slow, postsynaptic voltage dependent *N*-methyl-D-aspartate (NMDA) receptors ($\tau_{\text{NMDA}} = 150\ \text{ms}$, reversal potential 0 mV; Dayan and Abbott 2001; Gerstner and Kistler 2002), and therefore exhibit a superposition of conductance kinetics. The ratio of NMDA to AMPA receptors in a synapse was drawn from a Gaussian distribution with mean $\mu_{\text{NMDA/AMPA}} = 0.47$ and SD $\sigma_{\text{NMDA/AMPA}} = 0.2\mu_{\text{NMDA/AMPA}}$ (Myme et al. 2003).

Analogously, the inhibitory synaptic synapses were modeled as a mixture of GABA_A and GABA_B receptors. Whereas the GABA_A kinetic was again modeled as a relatively fast exponential decay ($\tau_{\text{GABA-A}} = 5\ \text{ms}$, reversal potential $-70\ \text{mV}$), the conductance kinetic of the GABA_B receptors was implemented according to a model proposed by (Destexhe et al. 1994) with parameter values taken from (Thomson and Destexhe 1999) (reversal potential $-90\ \text{mV}$). The GABA_B-to-GABA_A ratio of an individual inhibitory synapse was drawn from a uniform distribution between zero and a maximum ratio $m_{\text{inh}} = 0.3$.

INPUT MODEL. The electrophysiological recordings were done during presentation of natural movies. Although our modeling effort was concentrated on the V1 model, we needed a sufficiently realistic transformation of movie stimulus to (V1 input) spike trains. Therefore the retina and the lateral geniculate nucleus (LGN) were modeled, according to Dong and Atick (1995), as a spatio-temporal filter bank with nonlinearities, which seems to be a good compromise between simplicity and realism (Gazeres et al. 1998). The filter bank converted time varying input signals on the retina, such as movies, into firing rates of LGN neurons. Note that this feedforward, rate-based model neglects any feedback connections from V1 to LGN (Callaway 1998). Moreover, we neglected that the ganglion cells typically react to color opponency rather than to pure luminance differences (Perry et al. 1984). Thus the color movie was converted to a grayscale movie.

Retina model. The two-dimensional retinal inputs (movie frames) were filtered by “Mexican hat” (difference of Gaussians) spatial filters (Dong and Atick 1995; Enroth-Cugell and Robson 1966; Rodieck 1965). Filter sizes (describing the receptive fields of ganglion cells) were adapted to the geometry of parvocellular cells of macaque, where the SD of the Gaussian for center and surround were estimated to be $\sigma_{\text{center}} = 0.0177^\circ + 0.0019\varepsilon$ and $\sigma_{\text{surround}} \approx 6.67\ \sigma_{\text{center}}$ at eccentricity ε , respectively (in visual degrees; estimated from Fig. 4,

A and B in Croner and Kaplan 1995). After the convolution of the stimulus luminance portrait with these kernels (yielding S_{center} and S_{surround}), the response of a retinal ON-cell at visual field position r can be described by

$$R_{\text{ON}}(r) = C(r)[S_{\text{center}}(r) - \omega S_{\text{surround}}(r)]_+ \quad (2)$$

Following Croner and Kaplan (1995), we set the ratio of center to surround $\omega = 0.642$. The positive part of the center and surround interaction (indicated by the brackets $[\dots]_+$) was assigned to the response of an ON-cell and, analogously, the absolute value of the negative part to the response of an OFF-cell (Dong and Atick 1995). For simplicity, we assumed that the origins of the center and surround summation fields are identical, although a recent study suggests that there might be an offset between them (Conway and Livingstone 2006).

Applying the Difference-of-Gaussians model to the luminance of a stimulus results in a quantity called “contrast gain” (Croner and Kaplan 1995; Enroth-Cugell and Robson 1966; Rodieck 1965). To calculate the firing rate of ganglion cells, one has to multiply the “contrast gain” with the local contrast $C(r)$ (as done in Eq. 2) if one neglects nonlinear saturation in the high contrast regimen that is typically not reached for the natural stimuli we used here. Locality is important because the concept of a global contrast, easily defined for full-field grating stimuli commonly used in experiments, is not applicable for real world images and movies (Tadmor and Tolhurst 2000). Following Tadmor and Tolhurst (2000), we estimated the local contrast using the same kernels as

$$C(r) = \frac{|S_{\text{center}}(r) - S_{\text{surround}}(r)|}{S_{\text{center}}(r) + S_{\text{surround}}(r)} \quad (3)$$

where we additionally set the contrast to be zero in the case of darkness. Note that applying Eq. 3 results in a response $R_{\text{ON}}(r)$ that is sparser than for a constant global contrast, because the response is now quadratic in the center and surround luminance difference (see Eq. 2).

LGN model. The retinal output was filtered by the LGN model using a temporal kernel. The temporal kernel combines a phasic (taken from Dong and Atick 1995) and a tonic component (as in Gazeres et al. 1998), i.e., $k_{\text{LGN}} = k_{\text{phasic}} + k_{\text{tonic}}$. It is for nonnegative times

$$k_{\text{phasic}}(t) = t(1 - \pi\omega_c t)\exp(-2\pi\omega_c t) \quad (4)$$

and

$$k_{\text{tonic}}(t) = A \exp(-t/\tau)/\tau \quad (5)$$

Parameter $A = 0.3$ is the fraction of tonic activation (with respect to the peak firing rate) for a given stimulus, integrated over a time window of $\tau = 15$ ms. Parameter $\omega_c = 5.5 \text{ s}^{-1}$ defines the shape of the phasic kernel (Dong and Atick 1995).

The positive parts and the absolute values of the negative parts of the temporal convolutions were assigned to nonlagged and lagged cells, respectively. Altogether, there are four different time-varying rate outputs, i.e., that of any combination of nonlagged or lagged cells in the LGN with either ON- or OFF-cells from the retina (Dong and Atick 1995). Following Gazeres et al. (1998), a so-called “switching Gamma renewal process” was used to convert these time-varying rates to spike trains. This process, which was suggested to fit experimental data from cat LGN X-cells (Gazeres et al. 1998), adopts a higher spike time regularity for high-input rates (≥ 30 Hz; regularity parameter $r = 5$) and switches to a Poisson process for low rates (< 30 Hz). The spontaneous background activity of each LGN neuron was set to a low value of 0.15 Hz. The peak LGN spike rate f_{max} was adjusted to achieve a mean firing rate of about 7 Hz under movie stimulation, when the four input channels were combined. The 7-Hz mean rate was estimated from our electrophysiological data from

macaque monkey. Applying a typical 50-s movie section, we found that a mean rate of 7 Hz was achieved for $f_{\text{max}} = 250$ Hz. The peak response would be evoked by a dot of highest contrast filling the center region of a ganglion cell with optimal duration. This value is in good agreement with Gazeres et al. (1998), who reported peak rates range of 50–400 Hz.

Input connectivity to V1. The visual field is retinotopically arranged on the cortical surface. However, although there exists only one retinal ganglion cell per LGN cell corresponding to the same visual field position at all eccentricities in macaque, there is a considerable magnification in density of cortical neurons in V1 per degree of visual field (Schein and de Monasterio 1987; Tootell et al. 1982). Comparing several earlier studies, Schein and de Monasterio (1987) estimated the cortical magnification factor (CMF) at eccentricity ε to be (in mm cortex per degree of visual field)

$$\text{CMF} = \frac{12.2 \text{ mm}}{\varepsilon + 0.95^\circ} \quad (6)$$

This definition of the cortical magnification factor (Eq. 6) is very convenient: for a fixed eccentricity and distance between adjacent neurons (grid spacing), one can calculate the lateral extent of the network needed to cover a given visual field size. Note, however, that this estimate is only useful when the lateral extent of the network model can be regarded as small compared with the variation in lateral cell density.

LGN neurons, belonging to the parvocellular pathway, typically project to layer 4C β of V1. There is still an ongoing debate to which extent oriented input shapes the orientation selectivity of neurons in the primary visual cortex or to what extent local cortical processing is involved (see Teich and Qian 2006 for a review). It seems that in macaques, orientation selectivity is thought to arise from the interaction of cells with gradually shifted input characteristics across the sublamina of the layer 4C (Callaway 1998; Lund et al. 2003), whereas the inputs to a single cell might not be oriented in macaques as suggested for the cat (Hubel and Wiesel 1977). However, because we did not model sublamina, we simplified the circuitry by, nevertheless, assuming that input connections to each neuron generate orientation tuning. This allows the definition of orientation maps in a straightforward “hard-wired” manner in our model. We used Kohonen’s Self-Organizing Map algorithm (Kohonen 1982) to create orientation maps across the cortical surface, which is known to generate orientation maps with good correspondence to V1 orientation maps (Brockmann et al. 1997; Erwin et al. 1995; Obermayer and Blasdel 1993; Obermayer et al. 1990, 1992). See Fig. 1C for a typical orientation map generated by this algorithm (see APPENDIX A for details on the implementation of the algorithm).

Based on the generated orientation preferences for each cortical position, the thalamic input connection probability to a cell in the circuit could thus be modeled as an oriented Gabor function, i.e., a two-dimensional Gaussian multiplied by a cosine function. The absolute value of the Gabor function corresponds to the connection probability of LGN neurons with a cortical cell positioned at the cortical equivalent position of the origin of the Gabor patch in the visual field. Positive and negative regions correspond to the connection probabilities of LGN ON- and OFF-response cells, respectively. Lagged and nonlagged cells connected equally likely to cortical cells. Following Troyer et al. (1998), we expressed the Gabor function in parameters defining the number of subregions n_s , the aspect ratio of the width and the height of the Gaussian envelope a , the orientation φ , the offset of the cosine ψ , and the frequency of the cosine f . Given these parameters, one calculates the SD of the Gaussian envelope as (Troyer et al. 1998)

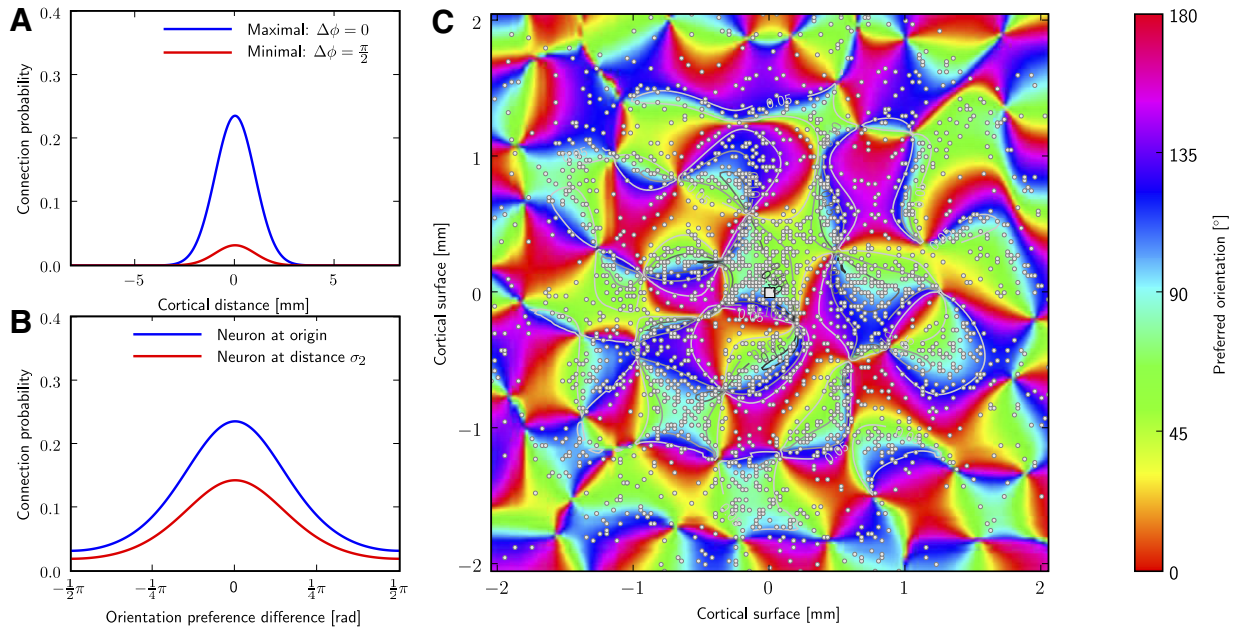


FIG. 1. Long-range connectivity of the V1 model. Long-range patchy connectivity of an example neuron implemented in a model circuit having $165 \times 165 \times 3$ neurons in layer 2/3 positioned on a cuboid grid with a spacing of $25 \mu\text{m}$. (Note, these dimensions are different from that used in the simulations of RESULTS; they are used here for better visualization). *A* and *B*: conditional probability that the neuron (marked with a white square in the center of *C*) is connected to a neuron having lateral distance r or orientation selectivity φ , respectively. The connection probability to a postsynaptic neuron at 0 lateral distance and same orientation preference was scaled to experimental data ($\approx 0.24\%$; Thomson et al. 2002). Blue and red curves show the connection probabilities for neurons that have aligned or orthogonal preferred orientation to the presynaptic neuron, respectively. *C*: connections established according to the probability distributions for a presynaptic neuron in the origin of the circuit (white square). Small white dots represent lateral positions of postsynaptic neurons. Colors code for orientation tuning of a neuron (generated by a self-organizing map). The conditional connection probabilities are indicated by contour lines. One notes that the connection probability rises for regions with similar orientation as the presynaptic neuron ($\sim 90^\circ$), thereby generating a patchy appearance. Only the orientated (long-range) part of Eq. 1 (2nd term) is used for establishing connections in this example plot. However, because the weighting factor is high $m = 10$ (see Eq. 1), only very few local connection will be added when considering both terms in the simulations. The orientation map additionally determines the orientation of thalamic input connections.

$$\Sigma^{1/2} = \frac{1}{9.792 f} \begin{pmatrix} n_s & 0 \\ 0 & a \end{pmatrix} \quad (7)$$

while using coordinates rotated by φ . The advantage of using these parameters is that the frequency defines implicitly the size of the Gabor patch while the number of subregions is kept constant. Therefore the receptive fields of macaque V1, which are much smaller than those of the cat, can be easily included in this framework. We used data from Bredfeldt and Ringach (2002) and chose the frequency f from a Gaussian distribution with a mean of 3.7 deg^{-1} and a SD of 2.1 deg^{-1} (with an enforced minimum of 0.7 deg^{-1} and maximum of 8.0 deg^{-1}). The number of subregions n_s and phase shifts ψ were drawn from uniform distributions with ranges of (1.85, 2.65) and (0, 2π), respectively (experimental values from cat as in Troyer et al. 1998).

To incorporate the smooth maps of preferred orientation φ and orientation preference q depending on cortical position u (see APPENDIX A), we set $\varphi = \varphi(u)$ and the aspect ratio to $a(u) = (a_{\max} - a_{\min})q(u) + a_{\min}$. We used values reported by Troyer et al. (1998) for the bounds $a_{\min} = 3.8$ and $a_{\max} = 4.54$ for excitatory neurons and for the generally less well-tuned inhibitory neurons, $a_{\min} = 1.4$ and $a_{\max} = 2.0$.

Last, the overall connection probability defined by the Gabor functions, was scaled to achieve an average number of 24 input synapses for both excitatory and inhibitory neurons, which is the estimated number of parvocellular afferent connection per cortical neuron in layer 4C of macaques (Peters et al. 1994). There is evidence that layer 6 receives occasional collaterals of the LGN input to layer 4 (Callaway 1998). Thus we set the connection probability to excitatory neurons in layer 5 (comprising layer 5 and layer 6 in our model) to 20% of that of the input to layer 4. These values are in good agreement with the data from Binzegger et al. (2004) estimated from

cat. In macaques, layer 2/3 receives only koniocellular input (Callaway 1998). Because we omitted the koniocellular pathway in our model, layer 2/3 did not receive any thalamic input.

Because of finite conduction velocities of the fibers, signals from the retina reach V1 with a characteristic delay of about 30 ms (Maunsell et al. 1999). We sampled the delay of the LGN input synapses from a Gaussian distribution with mean 31 ms and SD 5 ms (and additionally enforced delays below 24 ms and above 50 ms to a value uniformly in the latter range). These values were taken from Fig. 3 of Maunsell et al. (1999).

Top-down connections. In addition to the thalamic input, V1 neurons receive multiple feedback connections from extra-striate cortical areas (Felleman and Essen 1991), especially from V2, where the feedback connections are almost as numerous as the feed-forward connections (see Sincich and Horton 2005 for a review). Feedback projections predominantly project to targets in the upper layers but also to layer 5 (Rockland and Virga 1989; Sincich and Horton 2005).

Because our model is restricted to V1 and we do not have any recordings from V2 available, we decided to not include any top-down input stream explicitly. However, implicitly, additional input to V1 neurons is included by modeling the “high conductance state” of each neuron, which reflects the synaptic background input arriving from distal neurons (Destexhe et al. 2001).

Comparing the V1 model to electrophysiological data

SETUP OF THE STIMULUS TO THE MODEL. The stimulus, presented to the V1 model during simulation, resembled the one presented to the monkeys. We used a 10-s fragment of one of the movie segments (sw21) shown during the electrophysiological recordings as input movie for the model. However, modeling the whole $10 \times 7^\circ$ visual

field was not feasible because of computational costs. Therefore we trimmed the movie frames to a smaller size, covering $3 \times 3^\circ$ of the visual field. The center of the extracted region was aligned to the center of a receptive field of one of the electrodes (channel 7) of a particular session (“d04nm1”). Because the diameter of the receptive field of that electrode was experimentally determined to be 1.2° , the reduced stimulus should at least contain all direct input information available for neurons recorded by that electrode. On the retina, this receptive field was centered at $(0.69, -2.39^\circ)$ eccentricity relative to the fovea. In the model, we set the eccentricity, nevertheless, to 5° , because otherwise, the lateral extent (and, therefore the amount of neurons in the model) per visual degree would be prohibitively large (cf. Eq. 6). At 5° eccentricity, a V1 model covering $2.4 \times 2.4^\circ$ has a lateral extent of 5×5 mm cortical surface and neurons are positioned on a virtual grid of size $62 \times 62 \times 9$ if one assumes a lateral grid spacing of $80 \mu\text{m}$. Vertically, the grid spacing corresponds to $200 \mu\text{m}$. The visual field covered by the V1 model is somewhat smaller than the stimulus to avoid boundary effects in the input connectivity. For analogous reasons, the LGN neurons were set to cover an intermediate area of $3 \times 3^\circ$ (77×77 grid).

ESTIMATING THE RELATIVE STRENGTH OF THE THALAMIC INPUT. In the recorded spike trains, the mean firing rate of multiple trials (5-min duration) across monkeys and V1 electrode channels was on average 5.1 (4.8) Hz (SD) during movie stimulation and 1.9 (3.3) Hz during spontaneous activity (blank screen). Thus one could state that, because of the thalamic input, the mean firing rate of the circuit increases by about 3 Hz. From simultaneous extracellular recordings in LGN, we analogously find a mean firing rate of 7.1 (2.9) Hz during visual stimulation and 4.4 (2.1) Hz during absence of visual stimulation. Hence, in the LGN the movie stimulus increases the mean firing rate by about 60% of the spontaneous activity.

We used these values to determine the synaptic input weight scale ($W_{\text{In, scale}}$), i.e., the scaling factor of the peak conductances originating from LGN neurons, in the following manner: In the absence of all intercortical connections, the weight scaling factor of the input stream was set to a value achieving closest match to a given target mean firing rate in each neuron population (minimal Euclidean distance). Assuming that the main input drive to V1 (during visual stimulation) is from the thalamus, we set the target mean rate for the circuit to 2 Hz, which roughly corresponds to the activity increase seen during visual stimulation in our experimental data.

EVALUATING THE DEVIATION BETWEEN MODEL RESPONSE AND IN VIVO RECORDINGS. To compare the firing regimen of the model with that of the in vivo recordings we evaluated the discrepancy between a set of 10 statistical features calculated from the model response and the recorded spike trains (see APPENDIX B). After estimating a statistical feature on the experimental data and the model response, their deviation was calculated using Kulback-Leibler divergence or by calculated the mean squared error, depending whether the features resulted in an estimated probability distribution or not, respectively. This deviation was normalized by the average deviation seen in this features if tested between any two experimental sessions (different monkeys or different movie stimulus). We call this experimental data weighted deviation the normalized deviation (ND) for each statistical features. We report the normalized deviation averaged across all statistical features as a measure for the goodness of fit, and abbreviate it in the following with mean ND (MND).

Note that by construction a MND value of 1 indicates that the deviation between the model response and the in vivo data (average over all sessions) equals (on average over the 10 statistical features) the average deviation between individual experimental sessions. We used only one model random seed for the evaluation of the fitting error for each parameter setting to reduce computational costs.

To compensate for a lack of synaptic drive because of a much smaller neuron density in the model compared with reality, we introduce two scaling parameters $W_{\text{In, scale}}$ and W_{scale} . The $W_{\text{In, scale}}$

parameter, a multiplicative factor applied to all weights of the input connections, was set by a heuristic approach to approximately match the input strength observed in the experiments.

The second scaling parameter, the weight scale parameter W_{scale} , accounts for the recurrent synaptic drive adjustments and is a multiplicative factor applied to all recurrent weights. As this parameter is inherent to the model design, it cannot be constrained by literature values. Therefore to estimate the weight scale parameter W_{scale} , we used the value that minimizes the deviation of the model firing response statistics to the “statistical fingerprint” of the firing regimen of the in vivo recordings. To measure its deviation, we used the MND as described above. We restricted the analysis on the response of excitatory neurons only, because we expect that due to the generally larger size of excitatory neurons, the experimental recordings were strongly biased to record spikes originating from excitatory cells.

SIMULATION TECHNIQUES. All simulations were performed using the PCSIM simulation environment (Pecevski et al. 2009). It takes about 5 h on a quad core machine (2,664 MHz) to simulate the described model for 10 s of biological time (depending on the mean firing rate). All simulations were performed in a distributed fashion on a cluster of 30 such quad core machines.

RESULTS

We first established the “statistical fingerprint” of the spiking activity of the primary visual cortex (V1) under naturalistic stimulus conditions in vivo. The extracted statistical features provided the grounds for comparison with the simulated firing response of a detailed circuit model. Because we hypothesized that V1 works in a characteristic firing regimen favorable for its ongoing computations, we were particular interested in features possibly characterizing a computational advantageous regime. For instance, such a regimen might consist of highly irregular firing and low correlations between neurons (Brunel 2000; Legenstein and Maass 2007). We therefore extracted 10 salient statistical features, which are sensitive to various aspects of the spiking response, such as response strength, response variability, spike correlations, bursting behavior, and the possible usage of spiking codes with nonlinear dependencies on consecutive spike intervals (see APPENDIX B for exact definitions).

Statistical characterization of the spike response in vivo to movies in monkey area V1

We first analyzed electrophysiological recordings from V1 of anesthetized macaque monkeys during stimulation with natural movies. The data comprised spike responses measured in 10 sessions (from 4 anesthetized macaque monkeys), each with 12–40 repeated representations of a movie of 3.5–6 min length. In Fig. 2, *D* and *E*, typical spiking responses of selected neurons are depicted. We characterized the firing statistics of this experimental data using a set of 10 statistical features (Fig. 3). The same set of features were also used to characterize the model response as described below (Fig. 9). We found that spike responses of V1 under naturalistic stimuli conditions were typically highly variable over time and moderately low correlated between different neurons having a smooth fall-off for long time lags. Firing rate and burst rate distributions followed exponential distributions, burst size frequencies and ISI distributions exhibited a power-law structure. This described general picture is consistent with previous published values.

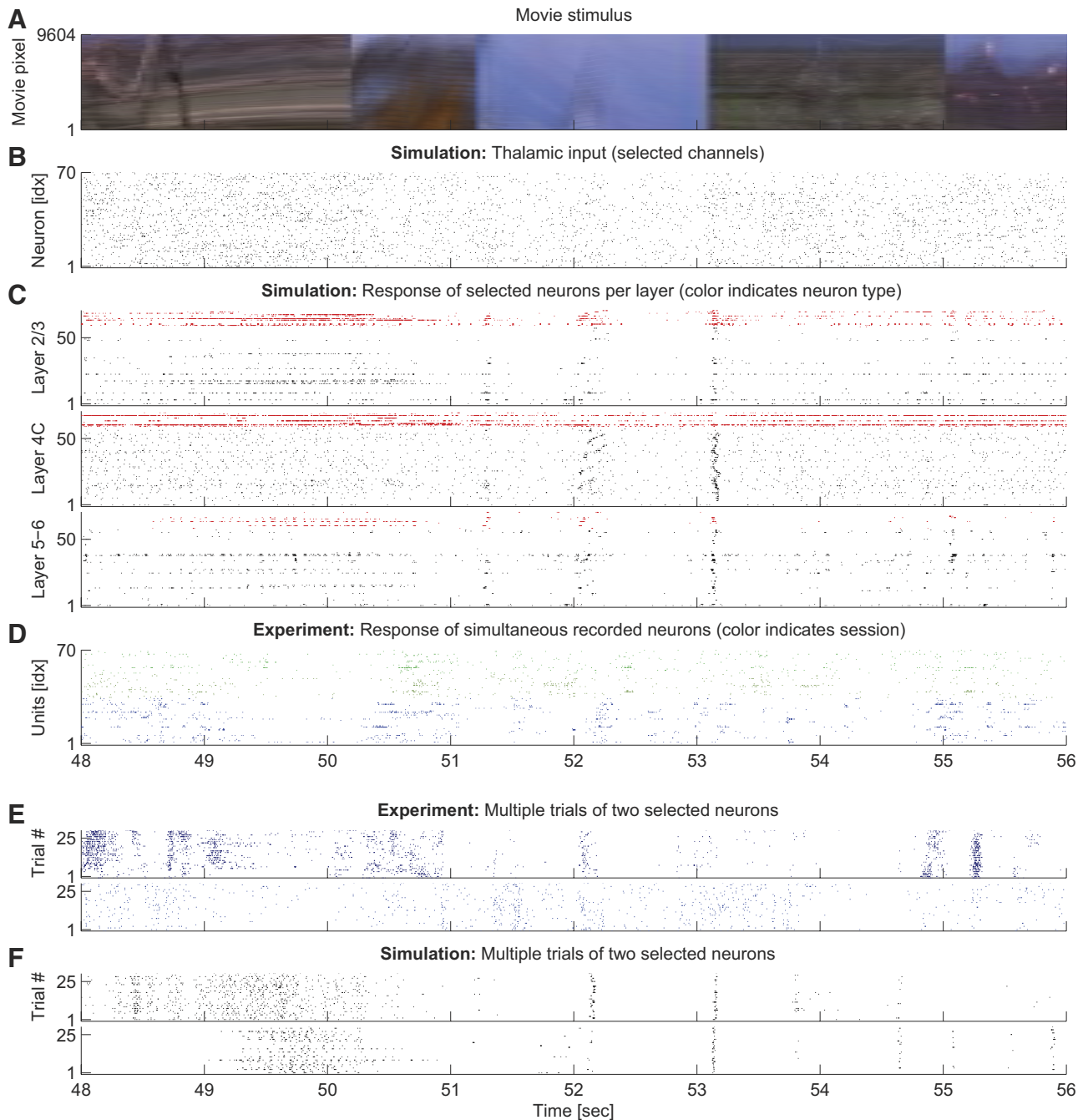


FIG. 2. Spiking response to movie stimulus in model simulation and in vivo. *A*: movie input to the model circuit in true colors (in the model, we used a grayscale version of this movie). Pixels of the movie frames are lined up vertically. *B*: lateral geniculate nucleus (LGN) model response to the movie in *A*. Seventy input channels were randomly selected for plotting (in total, there are 4,900 LGN inputs). *C*: spike trains elicited by neurons in the V1 model in response to the LGN output from *B* are plotted in separate panels for each of the layers 2/3, 4C, and 5–6. For better visualization, 70 neurons (of 11,532) are randomly chosen from each layer. Inhibitory and excitatory neurons are colored red and black, respectively. One notes a high variability in the statistical structure across neurons. *D*: spike trains of the spike sorted experimental data in response to the same movie segment are shown. Different colors represent different sessions of the same monkey—green (blue): 2 trials of session d04nm1 (d04nm2). We show 2 trials to allow for an easier comparison of the statistical structure of the spike trains in vivo with the model response (*C*). Note that the receptive field of some electrode channels lie outside of the depicted movie region of *A*. *E* and *F*: Multiple trials of 2 selected neurons in experiment (*E*) and model (*F*). Note that trial-to-trial variability is comparable in silico and in vivo.

In detail, the exponentially distributed firing rates (Fig. 3A) exhibited exponents varying between monkeys and experimental trials in the range of -2.35 to -0.23 s (mean -0.81 s, SD 0.62 s). The overall mean firing rate of the experimental data averaged over the different sessions was 5.06 ± 0.75 (SD) Hz.

The exponential distribution of firing rates is consistent with results from the V1 of cats (Baddeley et al. 1997).

Spike train variability is generally high. We tested for the variability in the spiking response using the distribution of Fano factors of individual neurons for multiple time scales

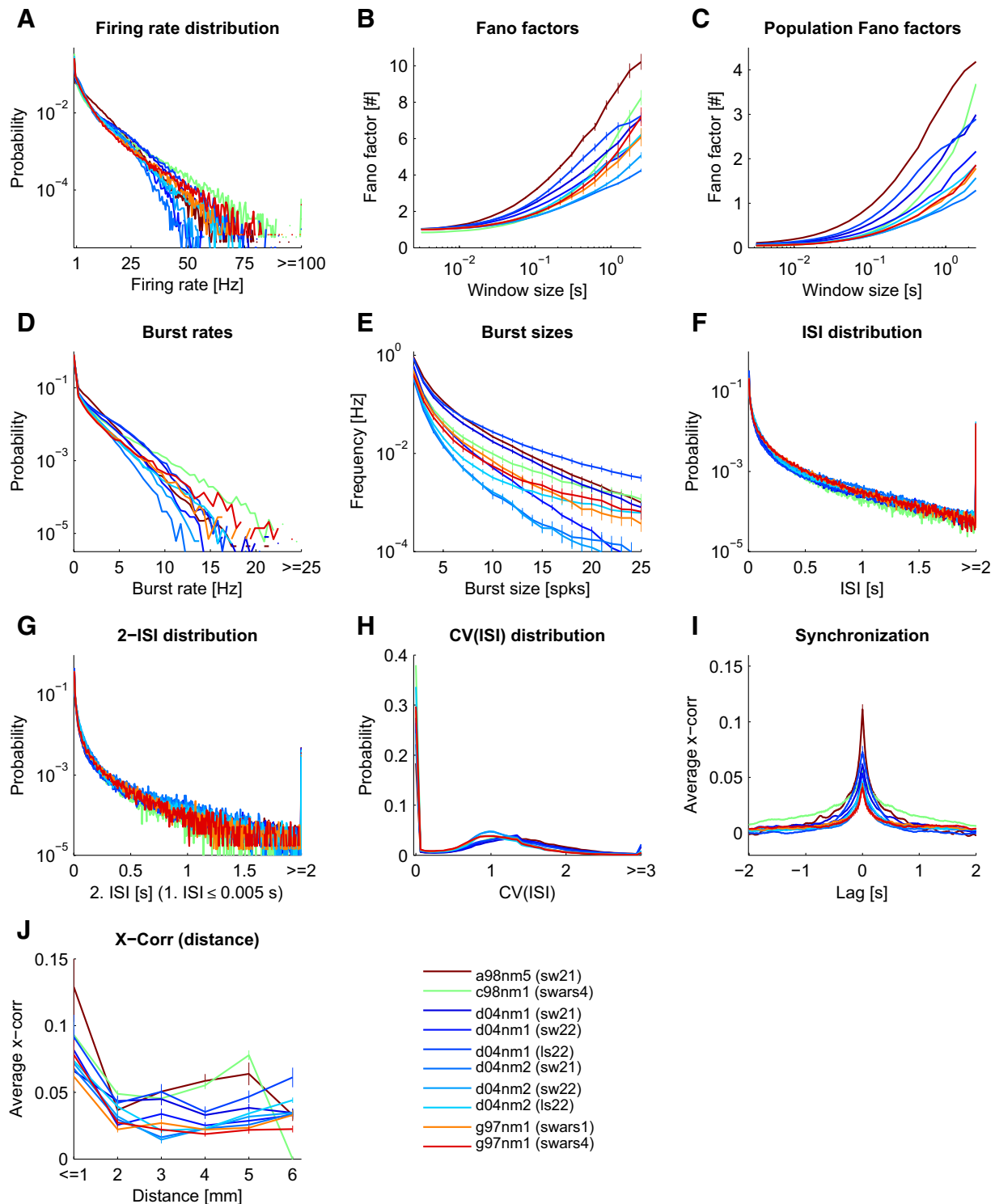


FIG. 3. Spike statistics of the experimental data. Each panel corresponds to a particular statistical feature (see APPENDIX B for exact definitions). Data from 10 experimental sessions (from 4 monkeys) during movie stimulation are plotted separately in color code (1st monkey, brown; 2nd monkey, green; 3rd monkey, shades of blue; 4th monkey, shades of red). In the legend, the 1st 3 letters of a session code indicate the animal, and the 2nd 3 letters indicate the recording session. The shown segment of the presented movie (Star Wars) is indicated in brackets. All available trials are included. Values greater than the plot limits were included in the last bin (where applicable), resulting in a disproportional large probability in the last bin. *G*: the conditional ISI distribution given that the 1st ISI is $<$ 5 ms. The full distribution is shown in *K* and *L*.

(Teich et al. 1997), and the Fano factor of the network population spike response, to measure the response variability of the population code. For individual neurons (Fig. 3*B*), the Fano factor approached 1 on average for small window sizes in

the order of 10 ms, indicating a Poisson process with stationary rates. On larger time scales, however, the Fano factor increased. This increase in variability could reflect the internal dynamics, but might be partly induced by the movie stimulus,

which mean brightness often varies on a time scale in the order of seconds.

The population Fano factor (Fig. 3C), measuring the response variability of the neuron population, showed a similar time window dependence as the Fano factor of individual neurons. However, the absolute value of the population Fano factor was markedly smaller, indicating that the population response was less variable over time on short time scales. On a longer time scale, however, the Fano factor of the population response increased, indicating that the neurons in the recorded population tend to be active or silent together. This might hint at population burst-like activity, also evident when examining the concrete spike trains in the recordings (see Rasch et al. 2008 for a discussion of how these clusters of spikes relate to the local field potential fluctuations in the same data).

The high variability of the *in vivo* data were also evident from the coefficient of variation of the interspike intervals [CV(ISI)], plotted in Fig. 3H. High probabilities were typically found for CV(ISI) values above 1, indicating a high variability in the spike response. Such a high peak value is consistent with previously published data (Holt et al. 1996; Shadlen and Newsome 1998; Softky and Koch 1993; Stevens and Zador 1998).

Spike bursts, i.e., abrupt events of high spiking activity, have been suggested to be an important aspect of neuronal coding of information. For instance, bursts might convey additional and independent information about the sensory inputs (Cattaneo et al. 1981; Lisman 1997). Thus we included two statistics to measure the occurrence of bursts in neuron spike trains, a feature rarely examined in the literature. Figure 3D shows the burst rate distribution, measuring the frequency of spiking events having at least two spikes within an (average) ISI of 5 ms. Figure 3E shows the average burst rate for different sizes of bursts (see APPENDIX B for exact definitions). Qualitatively, the burst rate distributions of different sessions looked similar, having exponential distributions. The exponent varied in the range of -5.07 s to -3.18 s (mean -4.54 s, SD 0.56 s). The average burst rate of all experimental data were 0.51 ± 0.17 (SD) Hz. However, in some sessions, there was a deviation from the exponential distribution and higher burst rates occurred more often than expected. Figure 3E shows that the burst rate as a function of the burst size can be described by a power law (a straight line in a log-log plot). We found exponents in the range of -3.52 to -2.29 (mean -2.88 , SD 0.43).

It is conceivable that a certain ISI distribution might be characteristic for the firing regimen of the cortex. ISI distributions (Fig. 3F) were very similar for different monkeys and different sessions. There was a high probability for the occurrence of long ISIs. The distribution of ISIs similarly followed a power law with an average exponent of -1.20 ± 0.19 (range from -1.47 to -0.98).

Additionally, to account for any local temporal correlations in the spike timings, we also estimated the two-ISI distribution, which is a two-dimensional distribution of the joint event of one ISI and the immediately following ISI (Fig. 3K). The ISI distribution for the following ISI when conditioned on a very short current ISI had a similar power-law shape as the marginal ISI distribution (Fig. 3G), although the occurrence of a short ISI following a short ISI was more likely. Similar to the full ISI

distribution, we found a relatively low variability across sessions and monkeys.

In general, we found that two neurons in V1 were on average correlated for lags up to about 250 ms having moderately low peak correlations. Other studies also reported low (signal) correlations between pairs of neurons for naturalistic stimuli (Reich et al. 2001; Yen et al. 2007) and even lower correlations in awake animals (Vinje and Gallant 2000). To be able to better compare our data to the literature, we calculated the shift-corrected cross-correlogram (Bair et al. 2001; Kohn and Smith 2005; Smith and Kohn 2008) and the noise correlations (r_{sc} ; Ecker et al. 2010) and found that the correlation structure in our data agreed very well with that of Smith and Kohn (Fig. 8). The strength of correlations however depended on the monkey and movie stimuli (Fig. 8, A and C). The mean value across all sessions was $r_{sc} = 0.26 \pm 0.03$ (SE) for neuron clusters nearer than 1 mm.

We further analyzed the cross-correlation for pairs of neurons as a function of their distance (Figs. 3J and 8A). In agreement with others (Smith and Kohn 2008), the cross-correlation was higher for neurons (clusters) recorded by the same electrode and decreased for longer electrode distances, where the correlation remained on a low level.

In summary, we computed a set of statistical features characterizing the “statistical fingerprint” of the spiking activity under seminatural movie stimulus condition *in vivo*. Certain features of the obtained fingerprint, namely the high variability of ISIs, low cross-correlation, and the power-law distributions of burst events, suggest that the V1 during movie stimulation might indeed reach an operating state, which is favorable for recurrent neural networks for performing computational tasks. The results presented here agree in general with published literature. However, because we characterized the firing regimen not only by a small set of mean values but instead by 10 different functions (or estimated probability distributions), we were able to quantify the deviation of the firing regimen of a simulated model from that exhibited *in vivo* in great detail. Moreover, the dataset provided us with the unique possibility to test the importance of physiological meaningful parameters to optimize the model response behavior to closely reach a realistic state.

Quantification of the discrepancy between the firing regimen of a model for a patch of V1 and the firing state exhibited in vivo

Having characterized the V1 *in vivo* recordings, we proceeded with characterizing the simulated responses of the circuit model of V1 *in silico*. The V1 model was based on anatomical and physiological details of macaque monkeys and was built to model the neural activation in a 5×5 -mm cortical patch of V1 (see METHODS for a detailed description of the V1 model). We simulated the model and recorded the spiking activity in response to 10 s of a typical movie segment (sw21) that had also been used for *in vivo* recordings.

Differences in the firing regimen *in silico* and *in vivo* were quantified by estimating the deviations in all statistical features. We calculated the MND between the model and the *in vivo* response (see METHODS for definitions). Note that MND = 1 indicates that the deviation of the model response to the mean response over all sessions equals the mean deviation between

TABLE 1. Parameters investigated in their optimization potentials together with their standard value by \mathbf{p}_{st}

| Parameter | Standard Value | Reference |
|------------------------------------------------------|----------------|------------------------|
| p_1 Noise level scale | 1.0 | (Destexhe et al. 2001) |
| p_2 Fraction of synapses with NMDA | 0.9 | |
| p_3 NMDA-AMPA ratio | 0.47 | (Myme et al. 2003) |
| p_4 Width of inh. connections, μm | 150.0 | (Lund et al. 2003) |
| p_5 Max. fraction of GABA _B conductance | 0.3 | |
| p_6 Inh. to exc. connections weight scale | 1.0 | (Thomson et al. 2002) |
| p_7 Exc. to inh. connections weight scale | 1.0 | (Thomson et al. 2002) |
| p_8 Long-range weight scale | 1.0 | |

Standard values for 5 of the parameters could be extracted from the literature. If no reference is given, the standard value was chosen heuristically.

all pairs of sessions. Our measure thus relates to the deviation among individual experimental sessions. Moreover, the MND weights the importance of each statistical feature in a manner that features showing a high variability between experimental sessions are deemed less important and those features conserved across sessions are emphasized.

By setting parameters of the model to values derived from the literature (Table 1) and minimizing the fitting error in respect to the overall recurrent connections weight scale, which is inherent to the model design (W_{scale} ; see METHODS), we found a mean normalized deviation of $MND = 1.91 \pm 0.01$ (mean \pm SE over identical networks and input but different random seed for the statistical evaluation), indicating that the deviation is on average about twice as high as between experimental sessions and monkeys.

Because we presented complex movie stimuli, it is not clear whether the firing regimen of the model was indeed generated by internal dynamics or was instead solely induced by the statistics of the input. To test the possibility of induced dynamics, we calculated the MND on the input spike trains generated by the LGN model (omitting the now meaningless lateral cross-correlation feature), and found a value of $MND = 2.49$. This value is considerably higher than for the model response. We repeated the statistical analysis for the model network after abolishing all recurrent connections, leaving only the input connections intact. By varying the strength of the synaptic input connections, we found a minimal value of $MND = 4.37$. Thus the fit of the firing statistics was much worse than with intact recurrent connections, implicating that the recurrent dynamics of the network indeed shaped the firing response.

We concluded that by simply optimizing an overall scale parameter (W_{scale}), the model dynamics shaped its statistical response properties in direction of that of the in vivo response. However, deviations from the realistic firing regimen in vivo were still considerable.

Improvement of the firing regimen when optimizing the model

Can the firing regimen of the model be adjusted by physiological meaningful parameters to improve the fit to the in vivo data? Finding such parameters would shed light on parameters that exert control over certain statistics. Therefore we chose

eight physiological meaningful parameters (see Table 1 for an overview), which we believed to influence the firing dynamics. We optimized the model in respect to each parameter and evaluated each parameter's ability to improve the discrepancy between model and in vivo recordings. Unfortunately, simultaneous optimization of multiple parameters was computationally prohibitive. Therefore we varied each parameter individually around the "standard" parameter values taken from the literature (\mathbf{p}_{st}), which we used to establish the initial fingerprint of the model's response (see above). Because the optimal W_{scale} might change during the variation of a parameter, we additionally varied W_{scale} resulting in two-dimensional landscapes (Fig. 5; see Table 2 for a summary of the quantitative results of the optimization). The effects of parameter optimizations on the improvement of each statistical feature are analyzed in Fig. 6.

We first chose a parameter varying the background noise strength (parameter p_1). The background noise strength implicitly regulates the strength of how neurons not modeled in the circuit affect the modeled neurons (see METHODS). When varying this parameter, we did not find a strong dependence on the quality of the fit (Fig. 5A), suggesting that this background noise strength was of minor importance. Although varying the noise strength improved some individual statistical features in respect to the literature values (such as Fano factors, burst sizes and ISI distributions; Fig. 6A), the effect was typically below 10% ND improvement. Indeed, even if we disabled the background noise, the fit to all statistical features simultaneously was only compromised by a negligible decrease of the MND of 3% (Fig. 6B). This suggests that our network was already big enough to explicitly provide realistic synaptic background inputs to any neuron.

In our model, the lateral width of inhibitory neurons was relatively small (SD 150 μm ; see METHODS). We tested whether the fit could be improved by varying the lateral spread of the inhibitory connections (p_4). However, this was not the case: a good range for this parameter lied between 150 and 250 μm , depending on the overall strength of the synapses (W_{scale} ; Fig. 5D). Although the ND of burst sizes and Fano factors could be markedly improved (Figs. 6A and Fig. 7), these features had only a small influence on the MND because their variance between experimental sessions was high and, moreover, they were already well fitted by a model with parameters set to standard values (cf. Fig. 7, right marginal plot). In consequence, the MND could only be improved by $\sim 5\%$ by optimizing the lateral connection width of inhibitory neurons, suggesting that our original value was adequate.

In general, we expected the synaptic receptor composition to be critical for achieving a realistic regimen. Because NMDA conductances are activated on a slow time scale and thus might affect the variability of the model especially on a longer time scale, we tested two parameters varying the amount of NMDA receptors in different ways: the fraction of synapses having NMDA receptors (p_2) and the average NMDA-to-AMPA ratio of a synapse (having NMDA receptors) (p_3). Knowing that the latter ratio shows a relatively high fluctuation in experimental literature (Myme et al. 2003) and that NMDA receptor function might be influenced by anesthesia (Guntz et al. 2005), these parameters might need to be adjusted in the model. Remarkably, when NMDA conductances were not included in the model at all, the fit degraded significantly (about 20%

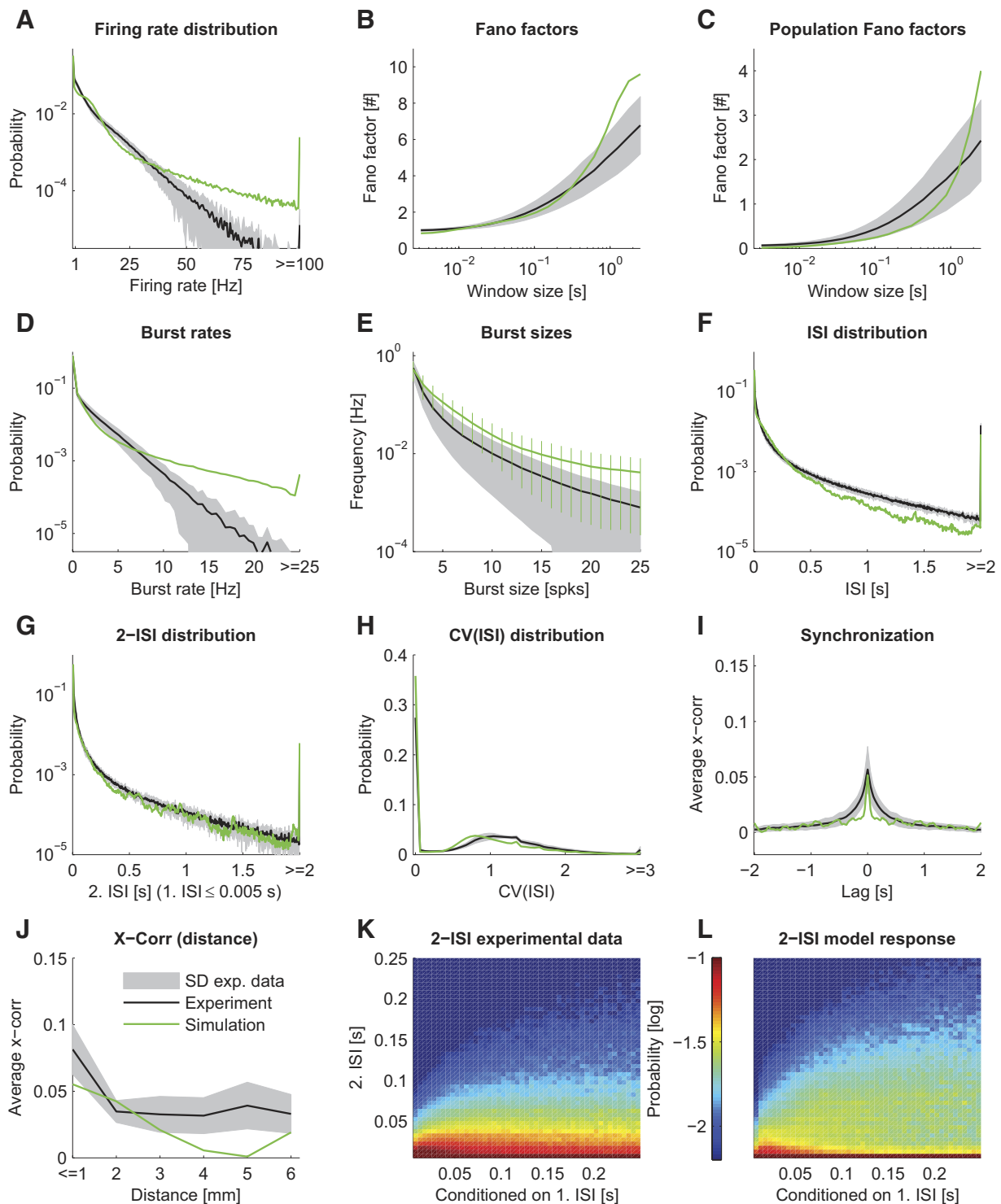


FIG. 4. The spike statistics of the model in comparison to the statistics of the in vivo recordings. The mean of the statistical feature estimated on the in vivo data are plotted as a black line. The gray area indicates the SD between different sessions. We used a 25-s part of the movie “sw21” as stimulus for the model. The spike statistics of the simulated model with optimized parameters (adjusted relative weight scaling factors of the patchy lateral long-range connections and of the connections from excitatory to inhibitory neurons) are plotted in green. The goodness of fit is mean normalized deviation (MND) = 1.10. Each panel corresponds to a particular statistical feature analogous to Fig. 3. Note that the 2-ISI distributions (K and L) are plotted conditioned on the 1st ISI.

decrease in MND), compromising mostly the fit to the ISI structure and the Fano Factors, but also the fit to the lateral cross-correlation (Fig. 6B). This suggests that the NMDA conductances were a necessary component of the network model to achieve a realistic firing regimen especially for the

variability on a longer time scale. However, we also noticed that varying these parameters led to only minor improvements (within 10% change of MND in respect to the standard parameters; Fig. 5, B and C). Thus we concluded that the standard literature values for the NMDA-to-AMPA

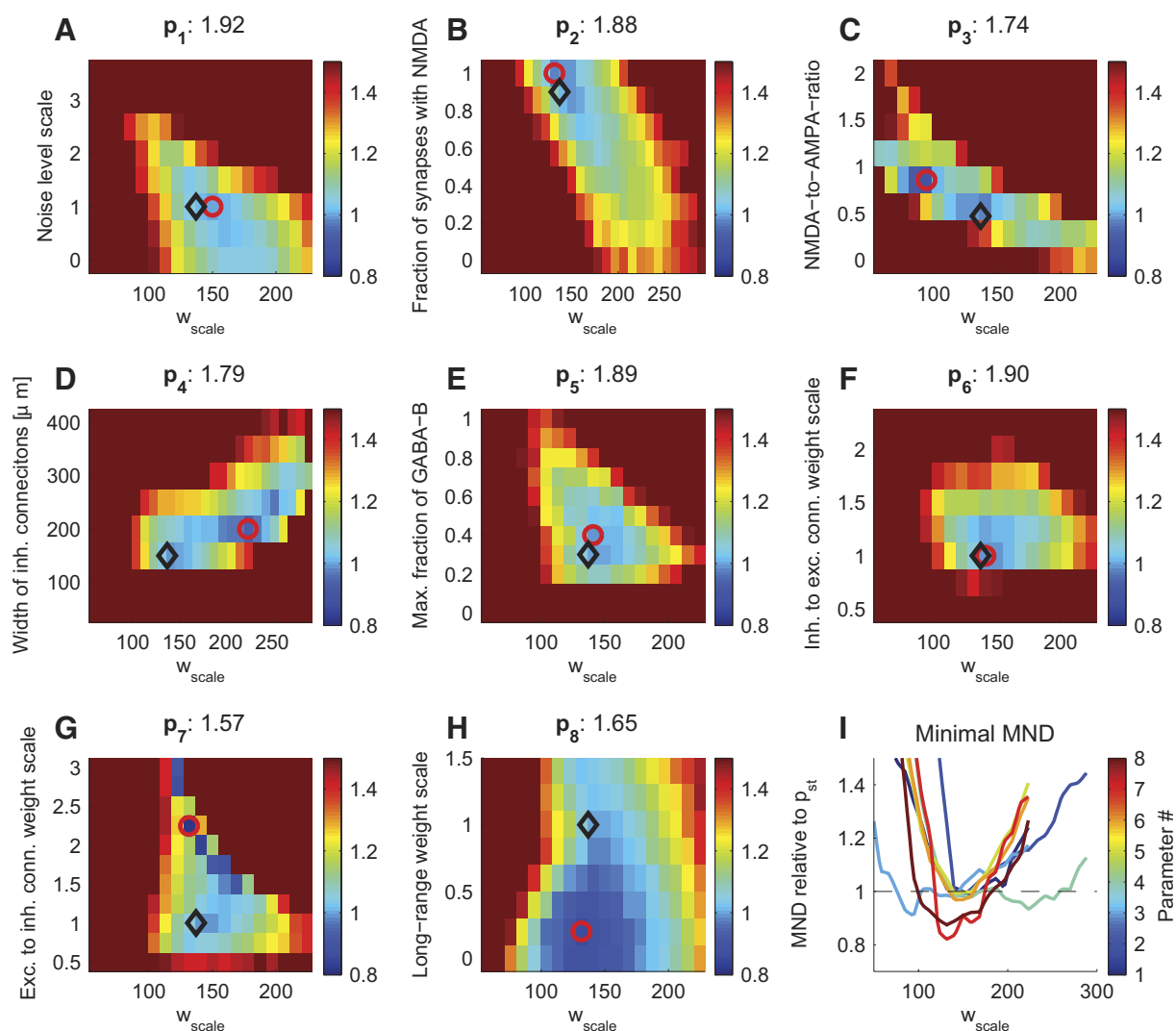


FIG. 5. Improvement in the goodness of fit between in vivo and in silico firing regimens when varying physiological meaningful general parameters. The improvement in MND in respect to the standard parameters is plotted in color code when varying 8 general parameters individually (see Table 1 for a description of the parameters). Each parameter was varied together with an overall scaling factor applied to all synaptic weights (W_{scale}), whereas other parameters were held constant. Adjusting some of the parameters considerably improved the fit to in vivo data. For instance, the relative synaptic weights of excitatory to inhibitory neurons needed to be increased dramatically (G). The standard parameter values and the settings showing the best fit in the statistical properties (minimal MND) are indicated with black diamonds and red circles, respectively. The minimal MND values are indicated in the titles. I shows the minimal MND (relative to standard parameters) vs. W_{scale} for the 8 parameters.

ratio and the fraction of synapses having NMDA receptors were already adequately chosen.

GABA_B conductances are activated nonlinearly only in case of high presynaptic activity events (Thomson and Destexhe 1999) and furthermore exhibit relatively slow dynamics. We thus expected that the adjustment of the maximal fraction of GABA_B conductances (p_3) would affect the population spike structure. Indeed, we found that the GABA_B conductances were critical in our model: including these conductances in the model dramatically improved the fit (about 80% improvement; Fig. 6B). One possible reason for this dependence on GABA_B conductances could be the crucial lack of long-lasting inhibition or the lack of nonlinear activation of inhibitory neurons when GABA_B conductances were absent.

The strong effect suggested that sufficient activation of inhibitory neurons was necessary for achieving a realistic firing

state. However, similar to the NMDA conductances, varying the maximal fraction of GABA_B conductances did not considerably improve the MND value in respect to standard parameters (Fig. 5E).

One might hypothesize that the balance of excitation and inhibition was not established appropriately in the network model. To vary the overall connection strength between neuron pools, we chose relative synaptic weight scaling factors from inhibitory to excitatory neurons (p_6) and from excitatory to inhibitory neurons (p_7) as parameters. Whereas varying the inhibitory to excitatory connection strengths did not yield any overall improvement (Fig. 5F), varying the reverse, the excitatory to inhibitory connection strengths had a strong effect. We noticed that increasing p_7 2.25-fold resulted in an 18% improvement of the fit to in vivo data (Fig. 5G), indicating the importance of correctly balancing inhibition and excitation for acquiring a realistic firing regimen. Judging from

TABLE 2. *Optimized parameter values*

| Parameter | Standard Value | Best Value | 5% Range Around Best Value | Corresp. W_{scale} | MND | |
|-----------|------------------------------------------------|------------|----------------------------|-----------------------------|-------|------|
| p_1 | Noise level scale | 1.00 | 0.76 | 0.42–1.10 | 160.4 | 1.92 |
| p_2 | Fraction of synapses with NMDA | 0.90 | 0.95 | 0.78–1.13 | 156.5 | 1.88 |
| p_3 | NMDA-to-AMPA ratio | 0.47 | 0.86 | 0.73–0.98 | 107.4 | 1.74 |
| p_4 | Width of inh. connections, μm | 150 | 208 | 182–233 | 223.8 | 1.79 |
| p_5 | Max. fraction of GABA _B conductance | 0.30 | 0.40 | 0.25–0.56 | 150.8 | 1.89 |
| p_6 | Inh. to exc. connections weight scale | 1.00 | 1.11 | 0.96–1.27 | 151.5 | 1.90 |
| p_7 | Exc. to inh. connections weight scale | 1.00 | 2.25 | 2.14–2.36 | 146.1 | 1.57 |
| p_8 | Long-range weight scale | 1.00 | 0.11 | 0–0.46 | 139.3 | 1.65 |

The best value (and the corresponding W_{scale}) for each parameter were inferred by grid search (see Fig. 5). The “5% range” indicates the range where the MND changed by at most 5% (in respect to its best value) and was estimated using a quadratic fit around the best value (with fixed W_{scale}). MND, mean normalized deviation.

the discontinuity of the error landscape (Fig. 5G), twofold increase in p_7 seemed to switch the firing regimen into a new state, which was much more similar to the firing regimen in nature.

This strong overall improvement in the MND was mainly mediated by the ND improvement in the correlation structure (lateral cross-correlation and synchronizations), which could be improved by about 40% in comparison to the simulation using standard literature values (Fig. 6A). Additionally, deviations in firing rate distribution and both Fano factors were also decreased by high percentages (Fig. 6A).

Finally, we chose the relative synaptic weights scaling factor of the patchy lateral long-range connections (p_8) because it is not well constrained by the literature (see METHODS for details). We found that the initial weight scale was somewhat too high: decreasing the weight of the long-range connections improved the variability of the network response. Indeed, the removal of long-range connections decreased the MND only by 3% (Fig. 6B). The decrease of the MND by 14%, when optimizing for the relative strength of the long-range connection (Fig. 5H), was mainly mediated by improving the burst structure (>50% improvement in the burst sizes and the burst rate distribution), as well as the CV(ISI) distribution (~35%; Fig. 6A). When inspecting the spike responses visually, we noticed a slow rhythmic bursting for high p_8 values (near 1). These periodic population bursts were not seen after decreasing p_8 . The

relative weight of the lateral long-range connections therefore had to be reduced to avoid the induction of population bursts resulting in a much better fit to responses in vivo, in particular reducing the deviation in the statistical features sensitive to the burst structure.

In summary, for the majority of the selected parameters, its literature value could not be markedly improved. The improved MND deviated <5% from the MND values in case of standard parameters. An intermediate effect could be seen when varying the NMDA-to-AMPA ratio (p_3). Here the improvement with respect to the standard parameters reached 9%. The most striking improvement, however, could be gained by varying the relative weight scaling factors of the long-range connections (p_8) and of the excitatory to inhibitory connections (p_7). Here the MND improved by 14 and 18%, respectively.

Next, we tested whether the fit could be further improved by varying the combination of the two most promising parameters together, i.e., the relative weight factors of excitatory to inhibitory connections and of patchy long-range connections, respectively, p_7 and p_8 . By setting p_7 to its best value (2.25) and again varying p_8 (as in Fig. 5H), the goodness of fit improved further to MND = 1.19 (for $p_8 = 0.3$). We simulated this optimized model for multiple trials (changing the random seed of the simulation) and found a mean MND value of $1.30 \pm$

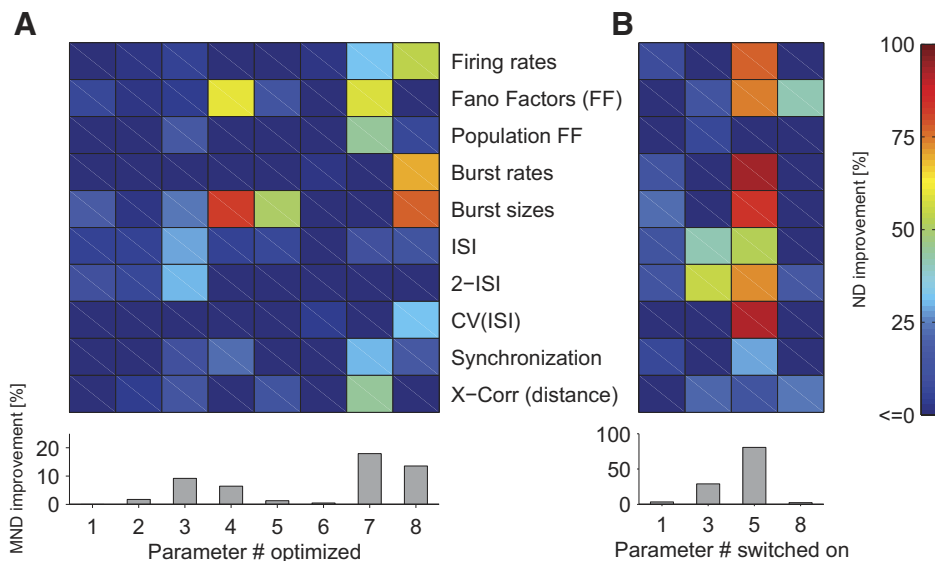


FIG. 6. Effects of parameter optimization on individual statistical features. **A**: the percentage change in normalized deviation (ND) in respect to standard parameter settings when optimizing parameters p_1, \dots, p_8 individually is plotted in color code (see Table 1 for a description of the parameters). One notes that individual parameters have different influences on statistical features. The bottom margin shows the improvement in MND (averaged over all statistical features). Same simulation data as in Fig. 5. **B**: impact of the inclusion of different components in the model. Selected components of the model: background noise (p_1), NMDA conductances (p_2), GABA_B conductances (p_5), or patchy long-range connections (p_8). The improvements of the fit when including a component are plotted in color code (relative to the standard parameter settings, having all components included). One notes that including GABA_B conductances had the most pronounced effects, improving the fit to multiple statistics profoundly. When components were switched on and off, W_{scale} was again optimized in respect to MND.

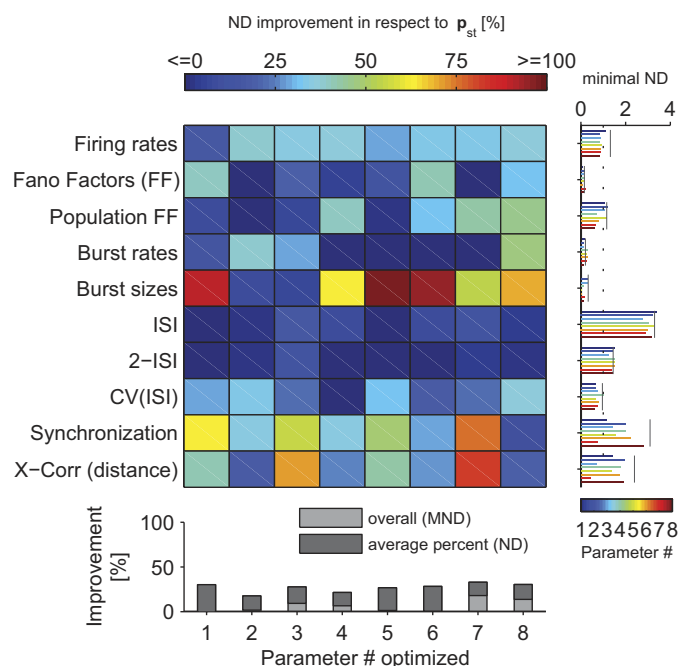


FIG. 7. Optimization of statistical feature individually (compared with optimize the mean over all). The improvement in ND relative to the standard parameters is plotted in color code. The ND of individual statistical features was always optimized in respect to W_{scale} . Parameters (listed in Table 1) have different impact on statistical features. The bottom margin indicates the cumulative ND improvements and the improvements in MND (where W_{scale} is optimized on MND instead of ND). Left margin shows the actual ND values for each parameter (color coded bars). Note that an ND of 1 means a deviation equal to the average deviation between experimental sessions (and monkeys). Black lines are plotted in case of standard parameters. One notes that some statistical features were more difficult to fit, whereas others were less problematic (reaching a value well below 1).

0.01 (SE). This is a 32% improvement over the model using standard parameters.

Finally, if a longer, nonintersecting section of the movie (25 s) was tested with these optimized parameters, the MND value decreased to a value of 1.10. Varying other parameters while using the best value for p_7 did not further improve the fit (data not shown).

Are these improvements robust toward changes in the network structure? Because we used only one network to optimize the firing regimen to reduce computational costs, we have to test the robustness of our findings in respect to a change in the network instance, which is a network generated by changing the seed of the random number generator for building the connectivity structure but having the same parameters. Exemplarily, we tested whether 10 networks with different construction random seeds achieved similar fits for the case of adjusting parameter p_7 and p_8 . The goodness of fit generally depended somewhat on the particular network instance. We found an average MND value of 1.32 ± 0.09 (for different trials and different networks on the 25-s movie segment), when variables were initiated by the optimized parameters described above (and connection weights, time delays, etc. of individual neurons and synapses were drawn randomly from distributions specified by general parameters). In general, the MND values therefore remained very stable when changing the network instance. However, in one exceptional network instance, we observed an outlier value of $MND = 2.81$ for the same movie

section. To test whether the optimal parameters are different in case of this outlier network and whether it could be readjusted to a realistic firing regimen, we recomputed the optimization exemplarily for the parameter p_7 . We found that the overall shape of the fitness landscape was almost identical to the original network (Fig. 5G), except that we had to reduce the overall weight scale (from 146 to 131) to reach a good MND value of 1.41. Remarkably, the optimal value for parameter p_7 remained the same (2.25).

We conclude that the particular instance of the random network structure will commonly not have major influences as long as not too extreme weight configurations are drawn by accident. Therefore the amount of neurons in the network is large enough to sample over random instances of connection weights for individual neurons.

In conclusion, by comparing the model response statistics to in vivo data, the contribution of physiological meaningful parameters for achieving a realistic firing state could be shown, and the effect on statistical features was quantified. Individual statistical features and the overall fit could be robustly improved by varying selected parameters. It was most effective to adjust the synaptic weights of the lateral long-range connection and to balance inhibition and excitation by strengthening the connections from excitatory to inhibitory neurons. The optimal parameter values were generally robust across network instances. The optimized network achieved a mean normalized deviation of $MND = 1.10$ (calculated on a long movie section), which is remarkably close to the average deviation between experimental sessions. In addition, for achieving a realistic regimen, both NMDA and GABA_B conductances were crucially important components of the network model.

Deviations of the model response to the in vivo firing regimen

After having optimized the firing regimen of the model, how does the model response still deviate from the in vivo data? To illustrate the spike responses of the model (after improving parameters), we plotted its response to a section of the movie together with the in vivo responses (Fig. 2). The general appearances of in vivo and in silico responses were very similar: high activity periods were followed by low activity periods, bursts were induced by salient features in the movie, and trial-to-trial variability was comparable.

Figure 4 plots the statistical features for the optimized model (25-s movie presentation, $MND = 1.10$) together with the average over in vivo data. As the MND value already indicated, the overall correspondences were good, but deviations were still noticeable. In particular, there was a tendency that high-activity periods were overrepresented across neurons of the network, as can be seen in the tails of the firing rate and burst rate distributions (Fig. 4, A and D). A lack of long ISIs (>500 ms) was evident in the ISI distribution (Fig. 4F). This lack of long intervals was consistent across all performed parameter variations. In Fig. 7, we examined the improvement of the ND of individual statistical features when varying a parameter (in contrast to the improvement in MND, see Figs. 5 and 6). In fact, the ISI distribution is most difficult to fit to in vivo responses, as the best ND is only around 3, i.e., three times worse than the deviation between sessions on average (Fig. 7, right margin plot).

It seems that neurons *in vivo* can exhibit dynamics on multiple time scales in contrast to the model, which tended to be strongly active for certain times and just silent for others. This stronger dependence of one ISI on the following ISI in the model response can be observed in Fig. 4, *K* and *L*. If the current ISI was very short, *in vivo* and model responses matched very well, having a relatively high probability that the following ISI was also very short and an exponential fall-off for the probability of longer ISIs (Fig. 4*G*) that was described well by a power-law behavior (i.e., straight line in log-log plot, data not shown). However, for longer ISIs, *in vivo* and model responses qualitatively differed. We found that *in vivo*, the shape of the distribution for the following ISI did not change qualitatively for longer ISI if conditioned on the current ISI (despite a small increase of the probability for longer ISIs). In particular, the conditional probability had still a power-law shape implicating that the probability for an ISI below and ≤ 50 ms was relatively high regardless of the current ISI (Fig. 4*K*). In contrast, in the model responses, the shape of the distribution changed if conditioned on longer ISIs: if the current ISI was long (> 100 ms), either the next ISI was very short (< 10 ms), possibly belonging to the onset of a population burst, or the length of the next ISI had nearly uniform probability up to about 120 ms (Fig. 4*L*). Varying the parameters had little effect on the deviation of the two-ISI distributions; the strongest effect was exerted by the NMDA-to-AMPA ratio (p_3), reaching 13% improvement in respect to the standard parameters. This lack of structured variability on multiple time scales in the model response was corroborated by the systematic underrepresentation of periods of high CV(ISI) (Fig. 4*H*).

Finally, the synchronization between two neurons and the lateral cross-correlation were generally too low in comparison with our experimental data (Fig. 4, *J* and *K*). In particular,

synchronization between neurons on lags longer than 50 ms was much weaker (Fig. 4*J*, see also Fig. 8*D*), suggesting that dynamics on slow time scales were still lacking in the model.

The correlation structure was most effectively influenced by four parameters (Fig. 7): the strength of the background noise (p_1), the NMDA-to-AMPA ratio (p_3), the GABA_B fraction (p_5), and the relative weight of the excitatory to inhibitory connections (p_7). As expected, introducing synaptic dynamics on a longer time scale (p_3 and p_5) improved the synchronization structure. Background noise likely helps to smooth the sharp peak in the synchronizations. It is not immediately clear why the strongest improvement in the synchronization (76%) and the lateral cross-correlation (83%) was mediated by the increase of the strength of excitatory to inhibitory connections. We think that this strengthening of excitatory synapses onto inhibitory neurons might have recruited local negative feedback loops and thus initiated dynamics on intermediate and longer time scales.

In summary, analyzing the deviations of the statistical features in detail suggested that the response of the model was limited in reproducing the broad temporal range of the dynamics *in vivo*. Especially, abruptly switching from activity to silence, low probability of bursting, and the temporal correlation of neurons on a longer time scale were difficult to achieve.

DISCUSSION

In this study, we investigated network spiking activity from the primary visual cortex under naturalistic stimulus presentation *in vivo* and *in silico*. We asked the question of whether a state-of-the-art connectionists' model is capable of reproducing the firing statistics observed *in vivo*, without any arbitrary

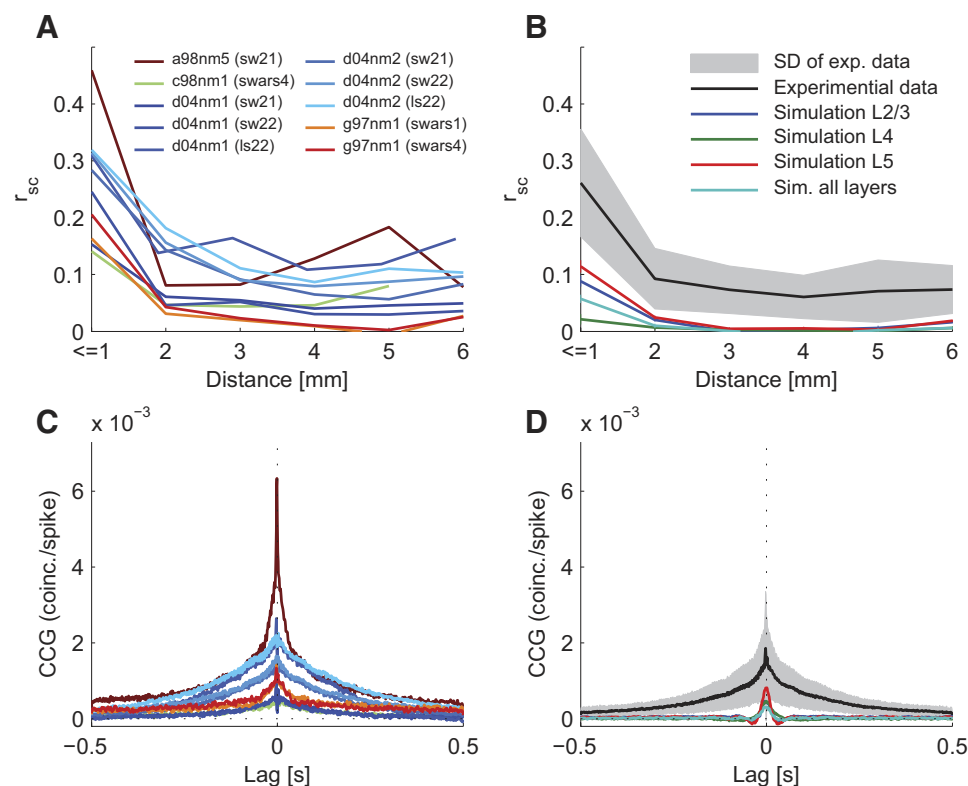


FIG. 8. Correlation structure in the model and *in vivo*. For better comparability with literature values, correlations were plotted in terms of noise correlations (*A* and *B*) and shift-corrected cross-correlograms (CCG; *C* and *D*). Sessions of experimental data were plotted as in Fig. 2 (*A* and *C*). *B* and *D*: the corresponding statistics calculated on the model response (for optimized parameter settings). Correlation structure in the model response were calculated on each layer separately showing a systematic difference in the strength of correlation in each layer (no layer information was available for the *in vivo* data). Correlations in the model were generally lower than in the *in vivo* data.

(unconstrained) adjustments of millions of variables, such as synaptic weights or temporal parameters of synapse dynamics.

We concentrated on characterizing the firing regimen of the primary visual cortex (V1), because it is an anatomically and physiologically well-studied cortical area. We characterized its firing regimen by extracting 10 statistical features from *in vivo* spike recordings from V1 of macaques under naturalistic stimulus conditions. We built and simulated a state-of-the-art circuit model reproducing a 5×5 -mm patch of V1 cortical circuitry and studied the discrepancy between the firing regimens of the simulated model and *in vivo* recordings.

The comparison showed that the firing regimen of the detailed laminar circuit model was comparable to *in vivo* recordings if parameters were set to values constrained by the literature. Responses were rich, showing high coefficient of variation of ISIs of individual neurons. We obtained a deviation averaged over all extracted statistics of about 2, meaning that the deviation was about twice as large as the average deviation between any two recording sessions.

We found that the deviation can be decreased dramatically (by 32%) if the relative synaptic weight of excitatory neurons to inhibitory neurons was increased more than twofold (compared with the literature values) and relative synaptic weights of the patchy long-range connections were adjusted to avoid slow rhythmic population activity. This indicates the importance of the balance of excitation and inhibition to achieve a realistic firing state in a network model.

We further found that selected physiological meaningful parameters affected statistical features of the response in a selective manner and that some ingredients of our network, such as the NMDA and GABA_B conductances, were crucially important for achieving a realistic firing state.

Evidence for a characteristic firing state in V1

This study does not answer whether there is indeed a computational advantageous firing regimen in neural tissue but instead tries to generally characterize a statistical fingerprint of spiking activity *in vivo* to compare the spiking activity to simulated responses *in silico*.

Our characterization of the firing statistics of *in vivo* responses generally agrees very well with findings of previous studies, which also used natural stimuli. We found some evidence that V1 might be in a characteristic state in anesthetized macaques. Our finding that the ISI distribution follows a power law is consistent with the ISI distribution of V1 cells of anesthetized cats and of IT cells of awake monkeys (Baddeley et al. 1997; Yen et al. 2008), as well as of neurons in motor cortex of awake rats (Tsubo et al. 2009). A power law distribution has partially been reported for *in vivo* spike data (Bedard et al. 2006) and the (spatial) size of neural avalanches (Beggs and Plenz 2003, 2004). Power law distributions have been conjectured on theoretical grounds as characteristic features of self-organized critical states in large complex systems (Jensen 1998). On the other hand, Bedard et al., (2006) reported that the ISI distributions derived from cat parietal association cortex during wakefulness and slow wave sleep show no evidence for power law behavior. This might indicate that the primary visual cortex and the parietal association cortex are working in different firing regimens.

There is still an ongoing debate on how strongly neighboring neurons are correlated, especially under natural conditions. Adding to this debate, Ecker et al. (2010) recently reported that, in awake and behaving monkeys, the spike count correlations r_{sc} are surprisingly low even between nearby neurons (in the range from 0.001 to 0.01). In our dataset, we found r_{sc} values of around 0.2 for different monkeys. Although one monkey showed very high correlations, which might be caused by some limited spiking cross-talk between nearby electrodes or spike-sorted clusters, in general, correlations are in agreement with the earlier studies and therefore stand similarly in contrast to the very low spike count correlations reported by Ecker et al. (2010). However, we have to emphasize that our acquisition technique used conventional arrays of single electrodes and the experiments were not specifically designed having this question of measuring spike correlations between isolated single neurons in mind. We therefore cannot add definite experimental arguments in this debate. However, we can say that in the optimized model the average spike count correlation was $r_{sc} = 0.06 \pm 0.01$ (SE) for nearby neurons (distances below 1 mm), which seems to support the very low values reported by Ecker et al. (2010).

Slow but largely irregular events of correlated activity cause the broad peak in the cross-correlation seen in our data (Fig. 8C) and were also reported by (Kelly et al. 2010). In the model it is possible to generate slow synchronous oscillatory activity with periods from hundreds of milliseconds to around a second by increasing the long-range lateral connection strength (p_8). This naturally raises the overall pairwise correlation between neurons. However, it turned out that the overall fit to the correlation function is worse in this oscillatory regimen because of the strong oscillatory component. Events of synchronous high activity of the *in vivo* data are much less regular than the population-burst like activity of the network model under these conditions. It is possible that these slow events in the experimental data reflect more global brain state dynamics observed under anesthesia (Kelly et al. 2010) and thus are impossible to achieve for our V1 model of relative restricted size.

However, the intralayer spike count correlation in the model response (plotted in Fig. 8, B and D) was very similar to recently reported layerwise recorded V1 data (Smith and Kohn 2009) in that it showed a very low correlation for layer 4, an intermediate correlation in deep layers, and the highest correlation within neurons from superficial layers. This hierarchy in correlation structure corresponds to the width of the lateral connections in the model and thus is likely induced by the lateral interactions between neurons.

Is the model in a realistic state?

We used recordings done in anesthetized macaques during the presentation of a commercial movie stimulus. In previous complementary studies, with participation of some of the present authors, these data have already been proven insightful in the analyses of information coding of the movie stimulus in the neural responses (Belitski et al. 2008; Montemurro et al. 2008) and in studying the relation of spikes to local field potentials (Rasch et al. 2008, 2009). We thus expect this dataset to be useful for describing a firing regimen under naturalistic stimulus conditions.

The firing regimen will likely depend on the current behavioral state of the animal. Because we used recordings from anesthetized animals, we characterized the firing regimen during anesthesia. Because most of the parameters constraining the model were not measured in behaving animals, the anesthetized state might actually be “more natural” for our network model. We expect that the firing regimen of awake and behaving animals will put stronger constraints on a current connectionist’s model to achieve.

Our model showed a good correspondence to our *in vivo* recordings. However, this does not necessarily implicate that the model would be able to perform any computational function of V1. In future studies, the next logical step toward a more realistic V1 model would therefore be to additionally include benchmarks on computational functions in the optimization process such as scatter of orientation tuning curves per layer or the emergence of complex cells in the superficial layers.

The good correspondence of our model to *in vivo* recordings also does not necessarily mean that the fit of the model to any kind of *in vivo* data could not in principle be improved further. We expect if more neurons could be simultaneously recorded, the deviations between model and experiment will increase because more constraints were set on the model design. Because of the small number of recorded neurons, our data were limited in the sense that we could only test whether our model does reproduce the general likeness of randomly selected neurons from V1. However, we argue here that benchmarking of network models of cortical areas to reproduce the general likeness is an important prerequisite to analyze realistic computational functions in network models and we outline in this article how this feat could be approached.

Given the diversity of cortical functions even within V1 (Ohlshausen and Field 2005), we assume that a computational advantageous firing regimen has to be quite general. We followed earlier setups of neural networks used for analyzing computational functions (Haeusler and Maass 2007; Maass et al. 2002) in that we draw synaptic weights and neuron to neuron connectivity from random distributions, without any specific learning of weights. Although the specific weight structure will influence the network response, we suppose that the general firing statistics will nevertheless be similar in a statistical sense if the network is not too specialized. Supporting this view, we found that different random seed in the network generation in general only slightly changed the goodness of fit. It is therefore a promising research direction to investigate self-organization of synaptic weights for instance by using an intrinsic plasticity rule to achieve a computationally advantageous firing regimen of recurrent networks (Schrauwen et al. 2008; Triesch 2007).

Because we extracted a number of different statistical features, measuring variability, correlation structure, and spike time dependency, it is likely that a hypothetical computational advantageous firing state of the cortex leaves its traces in the pool of extracted statistical features. Using a plethora of features has the advantage to minimize the bias of the investigator toward a particular aspect of the response. We also tested different error measures (such as a normalized mean squared error on the logarithm of the distributions instead of the Kullback-Leibler divergence), which slightly differed in the obtained optimal parameter values, because different as-

pects are deemed more important by other error measures (such as a good correspondence of the tail of the firing rate distribution). If there would be prior knowledge about the importance of statistical features, one could include this knowledge by changing the weighting for important features in the error measure (such as the deviation of the firing rate distribution from an exponential shape).

Which general parameters should be optimized in a cortical network model?

We developed a cortical network model for a 5×5 -mm patch of area V1. This model, consisting of about 35,000 neurons and 3.9 million synapses, was based on data from Thomson et al. (2002) regarding layer-specific connection probabilities and included short-term depression and facilitation of synaptic connections. Additionally, our model comprised data-based patchy long-range connections, two types of excitatory receptors (AMPA and NMDA), and two types of inhibitory receptors (GABA_A and GABA_B). The last years have seen several attempts to model large areas of the brain with similar components, such as inter- and intralaminar connectivity, laterally structured connectivity, synaptic depression and facilitation, and neurons having one or a few compartments (Izhikevich and Edelman 2008; Johansson and Lansner 2007; Kremkow et al. 2007; Tao et al. 2004). These models, as well as ours, incorporate many anatomical and physiological details, but they are, of course, still a strong abstraction of reality. Given the complexity of these models, it would be desirable to pinpoint a few general parameters that are sufficient to tune for achieving a realistic firing regimen. Then models could easily be adjusted, and studies of its computational functions could start from a realistic basis. Our analyses of optimizing a state-of-the-art cortical network model resulted in the following observations.

Most importantly, at the outset, the overall synaptic connection weight scale has to be adapted to account for the specific synaptic drive of each neuron, which is commonly lower in models because of the much smaller number of synapses. Furthermore, we had to adjust the relative weight of the patchy long-range connections to dampen the excitability of the network to avoid the tendency to produce periodic population bursts. This parameter was not well defined in the literature because synaptic contacts and weights of the long-range connections are unknown. We suspect that lateral interaction is tightly linked to computation in V1, and it is therefore likely that synaptic targets and weights are carefully selected by experience dependent learning mechanisms. Although we incorporated a higher probability for long-range connections toward similar orientated hypercolumns, our approach of drawing random weights is likely too unspecific in the target neuron selection. Thus long-range connections in our network might form a too generic source of excitation, which has to be damped to avoid rhythmic population bursts. On the other hand, the easiness of inducing periodic patterns on a very slow time scale (below 10 Hz and down to <1 Hz) by varying the overall strength of the lateral long-range connections in our network model indicates a possible mechanism for the generation of slow-wave activity commonly seen in the visual cortex and suggested to be important for information coding (Monte-murro et al. 2008).

In this study, the most effective parameter for tuning the model behavior was the relative synaptic weight scaling factor for the connections from excitatory to inhibitory neurons. To achieve a realistic regimen, we had to dramatically increase this parameter (>2-fold compared with literature values). Additionally, the fact that the GABA_B inhibition was crucially important further supports that inhibition has to be powerful enough over a long periods to cope with the excitatory drives. The necessity to increase the strength of inhibitory action in relation to literature values suggests that our implementation of the interaction between excitatory and inhibitory neurons underestimates the drive of inhibitory neurons in nature. Because our point neuron model ignores any spatial extent, dendritic and axonal tree architectures were not part of our model. However, it is known that dendrites are capable of nonlinearly integrate their synaptic inputs (Borg-Graham et al. 1998; Koch et al. 1983). For instance, some types of inhibitory neurons tend to target more soma proximal regions, whereas excitatory synapses are usually located in more distal parts of the dendritic tree (Markram et al. 2004). This arrangement gives rise to shunting inhibition (with appropriate reversal potentials, Koch et al. 1983), where inhibitory inputs nonlinearly overrule excitatory input. This mechanism effectively increases the strength of inhibitory action (compared with our point neuron model). It is likely that by increasing the weight of excitatory synapses on inhibitory targets in our model, the lack of nonlinear inhibition was partly compensated because inhibitory neurons were made more sensitive, which resulted in a more realistic state. We conclude that incorporating dendritic morphology (or other means to render the effect of inhibitory neurons more realistically) is a promising research direction and will likely improve firing states of network models.

Additionally, to keep the modeling effort tractable, many details of the primary visual system were neglected. For instance, the color processing pathways (Sincich and Horton 2005), motion processing pathways (dorsal stream), and a more accurate model of the LGN including feedback from V1 to the thalamus were not modeled. Whereas color and motion processing will only influence the movie features that are processed in V1, we expect the LGN to have more profound influences on the V1 firing state. For instance, it has been shown that irregular but correlated inputs to a neuron increase its CV(ISI) (Salinas and Sejnowski 2000; Softky and Koch 1993; Stevens and Zador 1998) and amplification of synchronous inputs caused by nonlinear interactions within dendrites further enhances the variability. Because the LGN is likely to deliver highly synchronous inputs to V1 (Wang et al. 2010) and furthermore might code information in bursts of activity (Reinagel et al. 1999), as well as because cortical feedback are known to induce thalamocortical spindle oscillations (Steriade et al. 1993), a more accurate LGN model may further improve the fit to in vivo data. Although we used a switching gamma process as a model for the LGN input and thus adopted special means to more realistically model episodes of high firing rates, the input still has independent Poissonian character for low firing rates. Our LGN model might not be realistic enough, in that generated spikes are less synchronous than in vivo (Wang et al. 2010).

In general, we noticed that variability of the dynamics on multiple time scale was still under-represented in our model. This was observable in the lack of high variability regions

[CV(ISI) distribution], the under-representation of long ISIs, and the too weak correlations between neurons spiking for lags >10 ms. It is therefore possible that our network is still not complex enough to generate a nonstereotyped long-lasting dynamics seen in vivo. Because we used point neurons models, neither compartmentization of dendrites nor dynamics of second messengers (such as calcium ions), nor any other cellular process were integrated in our model. The only processes reaching a time scale of a few hundreds of milliseconds in our model were slow synaptic conductances and synaptic short-term facilitation and depression. We suspect that dynamics of second messengers, which generally happen on a slower timescale than spike interactions, might be necessary ingredients for achieving a more realistic firing regimen (in particular on longer time scales).

Conclusion

The characterization of the in vivo response of neurons in monkey area V1 that we presented provides useful information for the investigation of large scale models for cortical areas. It is remarkable that a model for a patch of V1 that is solely based on previously published anatomical and physiological data produces (after adjusting a few general parameters) a spike response that matches the statistical properties of our in vivo data quite well. However, although similar in general statistical measures, we are still a long way of understanding the detailed neural coding properties of the cortex, which are manifested in the fine-structure of the interaction between neurons. The advent of techniques with the possibility to record from hundreds of neurons simultaneously will put forward new challenges for cortical network models. We expect that benchmarking models with in vivo data, as exemplified in this study, will foster the development of new and more realistic models for cortical areas, which will be important tools to ultimately understand neural functions.

APPENDIX A: ORIENTATION MAP GENERATION

It is well established that orientation preference and other features (such as visual field position, ocular dominance, or direction preference) form intertwined maps, where neighboring neurons tend to respond to similar features (Hubel and Wiesel 1977; Obermayer and Blasdel 1993). We used Kohonen's Self-Organizing Map algorithm (Kohonen 1982) to create orientation maps across the cortical surface. An orientation attribute was necessary for each neuron for defining thalamic inputs, as well as for preferred orientation dependent patchy lateral long-range connections. The algorithm has been used to generate feature maps, which resembled cortical measured feature maps in their overall appearance, as well as the occurrence of pinwheels (Brockmann et al. 1997; Erwin et al. 1995; Obermayer and Blasdel 1993; Obermayer et al. 1990, 1992).

Basically, the Kohonen's Self-Organizing Map algorithm tries to map a low-dimensional manifold (a horizontal sheet of neurons) to a high-dimensional feature space while ensuring that neighboring points on the manifold exhibit similar feature preference. Let $\mathbf{z} = [x, y, q \cos(2\varphi), q \sin(2\varphi)]^T$ define a feature vector, where $0 \leq x, y < k$ are the positions in visual space, $0 \leq q < 1$ is the orientation preference (or tuning strength), and $0 \leq \varphi < \pi$ is the preferred orientation. We did not model ocular dominance because our V1 model received input only from one retina. If one uses the low-dimensional variant of the learning rule (Erwin et al., 1995; Obermayer and Blasdel 1993), one attributes to each point on the manifold, i.e., each neuron having

cortical two-dimensional surface coordinates $u = (u_1, u_2)^T$, its current “optimal” feature vector $\mathbf{w}(u)$. Relations between neurons u and v are enforced by the neighborhood function $h(u, v) = \exp[-|u - v|^2 / (2\delta^2)]$. The update of the feature vector of a neuron v can be written as

$$\Delta \mathbf{w}(v) = \alpha h(u^*, v) [\mathbf{z} - \mathbf{w}(u^*)] \quad (8)$$

Note that in each learning step, the neuron u^* , showing maximal response to the current input \mathbf{z} , is updated in the direction of the input, weighted by a learning rate α . Depending on the cortical distance to the maximally activated neuron, the preferred features of the remaining neurons will be updated to a lesser extent in the same direction (mediated by the neighborhood function). In this rule, we took the maximally activated neuron to be the nearest in feature space to the current input, $u^* = \operatorname{argmin}_w |w(u^*) - \mathbf{z}|$. We sampled the input features from uniform distribution (within the above bounds). k regulates the hierarchy between different features (Obermayer et al., 1992) and was set to $k = 5$. If one starts from a retinotopic initial condition, a high value for k ensures that cortical position corresponds to visual space in an approximate one-to-one map. The characteristic length scale δ was set to match the experimental observed correlation length in cortical orientation maps (corresponding to the distance of neighboring pinwheel center) of $d_{\text{pin}} = 660 \mu\text{m}$ (Obermayer and Blasdel 1993). We used the approximate formula $\delta = \sqrt{k} d_{\text{pin}} / D / 8$, where D denotes the lateral extent of our V1 model.

APPENDIX B: STATISTICAL FEATURES

We defined 10 statistical features to characterize the spike train statistics. Each statistical measure was calculated on all available spike trains of the experimental session and the simulation, respectively. If not mentioned otherwise, we calculated the spike statistics using time windows with a length of 2 s. The time windows were overlapping with a step size of 0.2 s. The 10 chosen statistical features are the following:

Firing rate distribution

The distribution of mean firing rates in windows of 2-s duration.

Fano factor over different time scales

To characterize spike count variability over a range of time scales, we estimated Fano factors of the spike count distribution. These Fano factors are defined as the ratio of the variance to the mean of the spike-count distribution estimated over time windows of fixed length. We compared the average Fano factors for a range of time window durations (from $10^{-2.5}$ to $10^{0.4}$ s).

Population Fano factors

For different time windows (from $10^{-2.5}$ to $10^{0.4}$ s), we calculated the temporal mean spike count of the whole population of neurons and its variance. From these values, we calculated the Fano factors. These Fano factors describe the variability of the population firing rate.

Burst rate distribution

Burst events can be defined as having at least two spikes with an average ISI of ≤ 5 ms (Lisman 1997). The burst rate is the frequency of burst occurrence estimated within a period of time. The burst rate distribution describes the probability of different burst frequencies and was again estimated on time windows of 2 s duration.

Burst rates for different burst sizes

To analyze the occurrence of larger bursts, we calculated the burst rate distribution for burst events having at least n spikes with an average ISI of at most 5 ms. We took the average burst rates for a set of n minimal spikes ($n = 2 \dots 25$) as another statistical measure.

ISI distribution

This is the distribution of the intervals between two consecutive occurring spikes of one neuron. The distribution was estimated on the full length of the spike response to include longer intervals in the analysis. As before, we took all available trials and neurons to calculate a population statistic.

Two-ISI distributions

For neurons, placed in a recurrent network, the generation of a spike might depend in a systematic way on the relative timing of the previous spikes. To compare such dependencies, we estimated the two-ISI distributions. We define the two-dimensional two-ISI distribution $p(\tau_1, \tau_2)$ probability of occurrence of two sequential spike intervals of lengths τ_1 and τ_2 . These distributions were estimated on the full-length of the spike response.

ISI CV distribution

Another estimation of the variability of spike trains is the CV(ISI). The coefficient is defined as the ratio of the SD to the mean of the ISI distribution. The CV(ISI) was estimated on the available ISIs of each window of 2 s duration, and the resulting population statistics were taken for comparison. If there were less than three spikes in a given time window, we set the value of the CV(ISI) to zero.

Neuron synchronization

We defined synchronization as the mean cross-correlogram of spike activity between two neurons, which is the cross-covariance of the binned spike trains divided by the square root of the product of the variances (with a temporal bin size of 25 ms). We averaged over all spike clusters available in the sorted electrophysiological recorded spike trains and over 20,000 randomly drawn neuron pairs of the model circuit.

Spike time correlation as a function of distance

Lateral decorrelation of neural activity might be another important prerequisite for computational function of a neural circuit. Thus we calculated the cross-correlogram as a function of the Euclidean distance between two model neurons or recording sites. The temporal bin size was 50 ms and the spatial bin size was 500 μm . The correlation was averaged over time lags from -0.5 to 0.5 s.

ACKNOWLEDGMENTS

We thank M. Munk and C. Wang for comments and discussions.

GRANTS

This paper was written under partial support by the Austrian Science Fund (FWF) project S9102-N13, as well as Project FP6-015879 (FACETS), Project FP7-231267 (ORGANIC), and Project FP7-243914 (Brain-I-Nets) of the European Union, and the German Academic Exchange Service (program Modern Applications of Biotechnology in China).

DISCLOSURES

No conflicts of interest, financial or otherwise, are declared by the authors.

REFERENCES

- Adorjan P, Levitt JB, Lund JS, Obermayer K. A model for the intracortical origin of orientation preference and tuning in macaque striate cortex. *Vis Neurosci* 16: 303–318, 1999.
- Baddeley R, Abbott LF, Booth MCA, Sengpiel F, Freeman T, Wakeman EA, Rolls ET. Responses of neurons in primary and inferior temporal visual cortices to neural scenes. *Proc Biol Sci* 264: 1775–1783, 1997.
- Bair W, Zohary W, Newsome WT. Correlated firing in macaque visual area MT: time scales an relationship to behavior. *J Neurosci* 21: 1676–1697, 2001.
- Bartsch AP, van Hemmen JL. Combined Hebbian development of geniculocortical and lateral connectivity in a model of primary visual cortex. *Biol Cybern* 84: 41–55, 2001.
- Beaulieu C, Kisvarday Z, Somogyi P, Cynader M, Cowey A. Quantitative distribution of GABA-immunopositive and -immunonegative neurons and synapses in the monkey striate cortex (area 17). *Cereb Cortex* 2: 295–309, 1992.
- Bedard C, Kröger H, Destexhe A. Does the $1/f$ frequency-scaling of brain signals reflect self-organized critical states? *Phys Rev Lett* 97: 118102, 2006.
- Beggs JM, Plenz D. Neuronal avalanches in neocortical circuits. *J Neurosci* 23: 11167–11177, 2003.
- Beggs JM, Plenz D. Neuronal avalanches are diverse and precise activity patterns that are stable for many hours in cortical slice cultures. *J Neurosci* 24: 5216–5229, 2004.
- Belitski A, Gretton A, Magri C, Murayama M, Montemurro MA, Logothetis NK, Panzeri S. Low-frequency local field potentials and spikes in primary visual cortex convey independent visual information. *J Neurosci* 28: 5696–5709, 2008.
- Binzegger T, Douglas RJ, Martin KAC. A quantitative map of the circuit of cat primary visual cortex. *J Neurosci* 24: 8441–8453, 2004.
- Blasdel GG, Lund JS, Fitzpatrick D. Intrinsic connections of macaque striate cortex: axonal projections of cells outside lamina 4C. *J Neurosci* 5: 3350–3369, 1985.
- Blumenfeld B, Bibitchkov D, Tsodyks M. Neural network model of the primary visual cortex: from functional architecture to lateral connectivity and back. *J Comput Neurosci* 20: 219–241, 2006.
- Borg-Graham LJ, Monier C, Fregnac Y. Visual input evokes transient and strong shunting inhibition in visual cortical neurons. *Nature* 393: 369, 1998.
- Bredfeldt CE, Ringach DL. Dynamics of spatial frequency tuning in macaque V1. *J Neurosci* 22: 1976–1984, 2002.
- Brockmann D, Bauer HU, Riesenhuber M, Geisel T. SOM-model for the development of oriented receptive fields and orientation maps from non-oriented ON-center OFF-center inputs. In: *Artificial Neural Networks—ICANN'97. 7th International Conference Proceedings*, edited by Gerstner W, Germond A, Hasler M, Nicoud JD. Berlin: Springer-Verlag, 1997, p. 207–212.
- Brunel N. Dynamics of networks of randomly connected excitatory and inhibitory spiking neurons. *J Physiol Paris* 94: 445–463, 2000.
- Buzas P, Kovacs K, Ferecsko AS, Budd JML, Eysel UT, Kisvarday ZF. Model-based analysis of excitatory lateral connections in the visual cortex. *J Comp Neurol* 499: 861–881, 2006.
- Callaway EM. Local circuits in primary visual cortex of the macaque monkey. *Annu Rev Neurosci* 21: 47–74, 1998.
- Cattaneo A, Maffei L, Morrone C. Two firing patterns in the discharge of complex cells encoding different attributes of the visual stimulus. *Exp Brain Res* 43: 115–118, 1981.
- Chance FS, Nelson SB, Abbott LF. Complex cells as cortically amplified simple cells. *Nat Neurosci* 2: 277–282, 1999.
- Conway BR, Livingstone MS. Spatial and temporal properties of cone signals in alert macaque primary visual cortex. *J Neurosci* 26: 10826–10846, 2006.
- Croner LJ, Kaplan E. Receptive fields of P and M ganglion cells across the primate retina. *Vision Res* 35: 7–24, 1995.
- Dayan P, Abbott LF. *Theoretical Neuroscience: Computational and Mathematical Modeling of Neural Systems*. Cambridge, MA: MIT Press, 2001.
- Destexhe A, Mainen ZF, Sejnowski TJ. Synthesis of models for excitable membranes, synaptic transmission and neuromodulation using a common kinetic formalism. *J Comput Neurosci* 1: 195–230, 1994.
- Destexhe A, Rudolph M, Fellous JM, Sejnowski TJ. Fluctuating synaptic conductances recreate *in vivo*-like activity in neocortical neurons. *Neuroscience* 107: 13–24, 2001.
- Diesmann M, Gewaltig MO, Aertsen A. Stable propagation of synchronous spiking in cortical neural networks. *Nature* 402: 529–533, 1999.
- Dong DW, Atick JJ. Temporal decorrelation: a theory of lagged and non-lagged responses in the lateral geniculate nucleus. *Network Comput Neural Syst* 6: 159–178, 1995.
- Ecker AS, Berens P, Keliris GA, Bethge M, Logothetis NK, Tolias AS. Decorrelated neuronal firing in cortical microcircuits. *Science* 327: 584–587, 2010.
- Enroth-Cugell C, Robson JG. The contrast sensitivity of retinal ganglion cells of the cat. *J Physiol* 187: 517–552, 1966.
- Ernst UA, Pawelzik KR, Sahar-Pikielny C, Tsodyks M. Intracortical origin of visual maps. *Nat Neurosci* 4: 431–436, 2001.
- Erwin E, Obermayer K, Schulten K. Models of orientation and ocular dominance columns in the visual cortex: a critical comparison. *Neural Comput* 7: 425–468, 1995.
- Felleman DJ, Essen DCV. Distributed hierarchical processing in the primate cerebral cortex. *Cereb Cortex* 1: 1–47, 1991.
- Gazeran N, Borg-Graham LJ, Fregnac Y. A phenomenological model of visually evoked spike trains in cat geniculate nonlagged X-cells. *Vis Neurosci* 15: 1157–1174, 1998.
- Gerstner W, Kistler WM. *Spiking Neuron Models: Single Neurons, Populations, Plasticity*. Cambridge: Cambridge University Press, 2002.
- Gilbert CD, Das A, Ito M, Kapadia M, Westheimer G. Spatial integration and cortical dynamics. *Proc Natl Acad Sci USA* 93: 615–622, 1996.
- Girard P, Hupe JM, Bullier J. Feedforward and feedback connections between areas V1 and V2 of the monkey have similar rapid conduction velocities. *J Neurophysiol* 85: 1328–1331, 2001.
- Guntz E, Dumont H, Roussel C, Gall D, Dufrasne F, Cuvelier L, Blum D, Schiffmann SN, Sosnowski M. Effects of remifentanyl on N-methyl-D-aspartate receptor: an electrophysiologic study in rat spinal chord. *Anesthesiology* 102: 1235–1241, 2005.
- Gupta A, Wang Y, Markram H. Organizing principles for a diversity of GABAergic interneurons and synapses in the neocortex. *Science* 287: 273–278, 2000.
- Hausler S, Maass W. A statistical analysis of information-processing properties of lamina-specific cortical microcircuit models. *Cereb Cortex* 17: 149–162, 2007.
- Holt GR, Softky WR, Douglas RJ. Comparison of discharge variability in vitro and in vivo in cat visual cortex neurons. *J Neurophysiol* 75: 1806–1814, 1996.
- Hubel DH, Wiesel TN. Ferrier lecture. Functional architecture of macaque monkey visual cortex. *Proc R Soc Lond B Biol Sci* 198: 1–59, 1977.
- Izhikevich EM. Simple model of spiking neurons. *IEEE Trans Neural Netw* 14: 1569–1572, 2003.
- Izhikevich EM. *Dynamical Systems in Neuroscience: The Geometry of Excitability and Bursting (Computational Neuroscience)*. Cambridge, MA: MIT Press, 2006.
- Izhikevich EM, Edelman GM. Large-scale model of mammalian thalamocortical systems. *Proc Natl Acad Sci USA* 105: 3593–3598, 2008.
- Izhikevich EM, Gally JA, Edelman GM. Spike-timing dynamics of neuronal groups. *Cereb Cortex* 14: 933–944, 2004.
- Jensen HJ. *Self-Organized Criticality: Emergent Complex Behavior in Physical and Biological Systems (Cambridge Lecture Notes in Physics)*. Cambridge: Cambridge University Press, 1998.
- Johansson C, Lansner A. Towards cortex sized artificial neural systems. *Neural Netw* 20: 48–61, 2007.
- Kelly RC, Smith MA, Kass RE, Lee TS. Local field potentials indicate network state and account for neuronal response variability. *J Comput Neurosci* 29: 567–579, 2010.
- Koch C, Poggio T, Torre V. Nonlinear interactions in a dendritic tree: localization, timing, and role in information processing. *Proc Natl Acad Sci USA* 80: 2799–2802, 1983.
- Kohn A, Smith MA. Stimulus dependence of neuronal correlation in primary visual cortex of macaque. *J Neurosci* 25: 3661–3673, 2005.
- Kohonen T. Self-organized formation of topologically correct feature maps. *Biol Cybern* 43: 59–69, 1982.
- Kremkow J, Kumar A, Rotter S, Aertsen A. Emergence of population synchrony in a layered network of the cat visual cortex. *Neurocomputing* 70: 2069–2073, 2007.
- Legenstein R, Maass W. Edge of chaos and prediction of computational performance for neural microcircuit models. *Neural Netw* 20: 323–334, 2007.
- Lisman J. Bursts as a unit of neural information: making unreliable synapses reliable. *Trends Neurosci* 20: 38–43, 1997.
- Logothetis NK, Guggenberger H, Peled S, Pauls J. Functional imaging of the monkey brain. *Nat Neurosci* 2: 555–562, 1999.

- Logothetis NK, Merkle H, Augath M, Trinath T, Ugurbil K.** Ultra high-resolution fMRI in monkeys with implanted RF coils. *Neuron* 35: 227–242, 2002.
- Lund JS, Angelucci A, Bressloff PC.** Anatomical substrates for functional columns in macaque monkey primary visual cortex. *Cereb Cortex* 13: 15–24, 2003.
- Maass W, Natschläger T, Markram H.** Real-time computing without stable states: a new framework for neural computation based on perturbations. *Neural Comput* 14: 2531–2560, 2002.
- Markram H.** The Blue Brain Project. *Nat Rev Neurosci* 7: 153–160, 2006.
- Markram H, Toledo-Rodriguez M, Wang Y, Gupta A, Silberberg G, Wu C.** Interneurons of the neocortical inhibitory system. *Nat Rev Neurosci* 5: 793–807, 2004.
- Markram H, Wang Y, Tsodyks M.** Differential signaling via the same axon of neocortical pyramidal neurons. *Proc Natl Acad Sci USA* 95: 5323–5328, 1998.
- Maunsell JH, Ghose GM, Assad JA, McAdams CJ, Boudreau CE, Noerager BD.** Visual response latencies of magnocellular and parvocellular LGN neurons in macaque monkeys. *Vis Neurosci* 16: 1–14, 1999.
- McGuire BA, Gilbert CD, Rivlin PK, Wiesel TN.** Targets of horizontal connections in macaque primary visual cortex. *J Comp Neurol* 305: 370–392, 1991.
- Montemurro M, Rasch MJ, Murayama Y, Logothetis NK, Panzeri S.** Phase-of-firing coding of natural visual stimuli in primary visual cortex. *Curr Biol* 18: 375–380, 2008.
- Myme CI, Sugino K, Turrigiano GG, Nelson SB.** The NMDA-to-AMPA ratio at synapses onto layer 2/3 pyramidal neurons is conserved across prefrontal and visual cortices. *J Neurophysiol* 90: 771–779, 2003.
- Obermayer K, Blasdel GG.** Geometry of orientation and ocular dominance columns in monkey striate cortex. *J Neurosci* 13: 4114–4129, 1993.
- Obermayer K, Blasdel GG, Schulten K.** Statistical-mechanical analysis of self-organization and pattern formation during the development of visual maps. *Phys Rev A* 45: 7568–7589, 1992.
- Obermayer K, Ritter H, Schulten K.** A principle for the formation of the spatial structure of cortical feature maps. *Proc Natl Acad Sci USA* 87: 8345–8349, 1990.
- O’Kusky J, Colonnier M.** Postnatal changes in the number of astrocytes, oligodendrocytes, and microglia in the visual cortex (area 17) of the macaque monkey: a stereological analysis in normal and monocularly deprived animals. *J Comp Neurol* 210: 307–315, 1982.
- Olshausen BA, Field DJ.** How close are we to understanding V1? *Neural Comput* 17: 1665–1699, 2005.
- Pecevski D, Natschläger T, Schuch K.** PCSIM: a parallel simulation environment for neural circuits fully integrated with python. *Front Neuroinform* 3: 11, 2009.
- Perry VH, Oehler R, Cowey A.** Retinal ganglion cells that project to the dorsal lateral geniculate nucleus in the macaque monkey. *Neuroscience* 12: 1101–1123, 1984.
- Peters A, Payne BR, Budd J.** A numerical analysis of the geniculocortical input to striate cortex in the monkey. *Cereb Cortex* 4: 215–229, 1994.
- Quian Quiroga R, Nadasdy Z, Ben-Shaul Y.** Unsupervised spike detection and sorting with wavelets and superparamagnetic clustering. *Neural Comput* 16: 1661–1687, 2004.
- Rasch MJ, Gretton A, Murayama Y, Maass W, Logothetis NK.** Inferring spike trains from local field potentials. *J Neurophysiol* 99: 1461–1476, 2008.
- Rasch MJ, Logothetis NK, Kreiman G.** From neurons to circuits: linear estimation of local field potentials. *J Neurosci* 29: 13785–13796, 2009.
- Reich DS, Mechler F, Victor JD.** Independent and redundant information in nearby cortical neurons. *Science* 294: 2566–2568, 2001.
- Reinagel P, Godwin D, Sherman SM, Koch C.** The encoding of visual information by LGN bursts. *J Neurophysiol* 81: 2558–2569, 1999.
- Rockland KS, Virga A.** Terminal arbors of individual “feedback” axons projecting from area V2 to V1 in the macaque monkey: a study using immunohistochemistry of anterogradely transported *Phaseolus vulgaris-leucoagglutinin*. *J Comp Neurol* 285: 54–72, 1989.
- Rodieck RW.** Quantitative analysis of cat retinal ganglion cell response to visual stimuli. *Vision Res* 5: 583–601, 1965.
- Salinas E, Sejnowski TJ.** Impact of correlated synaptic input on output firing rate and variability in simple neuronal models. *J Neurosci* 20: 6193–6209, 2000.
- Schein SJ, de Monasterio FM.** Mapping of retinal and geniculate neurons onto striate cortex of macaque. *J Neurosci* 7: 996–1009, 1987.
- Schrauwen, B, Wardermann, M, Verstraeten, D, Steil, JJ, Stroobandt, D.** Improving reservoirs using intrinsic plasticity. *Neurocomputing* 71: 1159–1171, 2008.
- Shadlen MN, Newsome WT.** The variable discharge of cortical neurons: Implications for connectivity, computation, and information coding. *J Neurosci* 18: 3870–3896, 1998.
- Sincich LC, Horton JC.** The circuitry of V1 and V2: integration of color, form, and motion. *Annu Rev Neurosci* 28: 303–326, 2005.
- Smith MA, Kohn A.** Spatial and temporal scales of neuronal correlation in primary visual cortex. *J Neurosci* 28: 12591–12603, 2008.
- Smith MA, Kohn A.** *Lamina Dependence of Neuronal Correlation in Macaque V1*. Chicago, IL: Society for Neuroscience, 2009.
- Softky WR, Koch C.** The highly irregular firing of cortical cells is inconsistent with temporal integration of random epsps. *J Neurosci* 13: 334–350, 1993.
- Song S, Sjöström PJ, Reigl M, Nelson S, Chklovskii DB.** Highly nonrandom features of synaptic connectivity in local cortical circuits. *PLoS Biol* 3: e68, 2005.
- Steriade M, McCormick DA, Sejnowski TJ.** Thalamocortical oscillations in the sleeping and aroused brain. *Science* 262: 679, 1993.
- Stevens CF, Zador AM.** Input synchrony and the irregular firing of cortical neurons. *Nat Neurosci* 1: 210–217, 1998.
- Tadmor Y, Tolhurst DJ.** Calculating the contrasts that retinal ganglion cells and LGN neurones encounter in natural scenes. *Vision Res* 40: 3145–3157, 2000.
- Tao L, Shelley M, McLaughlin D, Shapley R.** An egalitarian network model for the emergence of simple and complex cells in visual cortex. *Proc Natl Acad Sci USA* 101: 366–371, 2004.
- Teich AF, Qian N.** Comparison among some models of orientation selectivity. *J Neurophysiol* 96: 404–419, 2006.
- Teich MC, Heneghan C, Lowen SB, Ozaki T, Kaplan E.** Fractal character of the neural spike train in the visual system of the cat. *J Opt Soc Am A Opt Image Sci Vis* 14: 529–546, 1997.
- Thomson AM, Destexhe A.** Dual intracellular recordings and computational models of slow inhibitory postsynaptic potentials in rat neocortical and hippocampal slices. *Neuroscience* 92: 1193–1215, 1999.
- Thomson AM, West DC, Wang Y, Bannister AP.** Synaptic connections and small circuits involving excitatory and inhibitory neurons in layers 2–5 of adult rat and cat neocortex: triple intracellular recordings and biocytin labelling in vitro. *Cereb Cortex* 12: 936–953, 2002.
- Tootell RB, Silverman MS, Switkes E, Valois RLD.** Deoxyglucose analysis of retinotopic organization in primate striate cortex. *Science* 218: 902–904, 1982.
- Triesch J.** Synergies between intrinsic and synaptic plasticity mechanisms. *Neural Comput* 19: 885–909, 2007.
- Troyer TW, Krukowski AE, Priebe NJ, Miller KD.** Contrast-invariant orientation tuning in cat visual cortex: thalamocortical input tuning and correlation-based intracortical connectivity. *J Neurosci* 18: 5908–5927, 1998.
- Tsubo Y, Isomura Y, and Fukai T.** Power-law distributions of inter-spike intervals in in vivo cortical neurons. In: *Frontiers in Systems Neuroscience*. Conference Abstract: Computational and Systems Neuroscience 2009. doi: 10.3389/conf.neuro.06.2009.03.320.
- Tyler CJ, Dunlop SA, Lund RD, Harman AM, Dann JF, Beazley LD, Lund JS.** Anatomical comparison of the macaque and marsupial visual cortex: common features that may reflect retention of essential cortical elements. *J Comp Neurol* 400: 449–468, 1998.
- Vinje WE, Gallant JL.** Sparse coding and decorrelation in primary visual cortex during natural vision. *Science* 287: 1273–1276, 2000.
- Vogels TP, Abbott LF.** Signal propagation and logic gating in networks of integrate-and-fire neurons. *J Neurosci* 25: 10786–10795, 2005.
- Wang HP, Spencer D, Fellous JM, Sejnowski TJ.** Synchrony of Thalamocortical inputs maximizes cortical reliability. *Science* 328: 106–109, 2010.
- Wenisch OG, Noll J, van Hemmen JL.** Spontaneously emerging direction selectivity maps in visual cortex through STDP. *Biol Cybern* 93: 239–247, 2005.
- Wieland DJ, Shelley M, McLaughlin D, Shapley R.** How simple cells are made in a nonlinear network model of the visual cortex. *J Neurosci* 21: 5203–5211, 2001.
- Yen SC, Baker J, Gray CM.** Heterogeneity in the responses of adjacent neurons to natural stimuli in cat striate cortex. *J Neurophysiol* 97: 1326–1341, 2007.
- Yen SC, Baker J, Lachaux JP, Gray CM.** Responses of primary visual cortical neurons to natural movies in anesthetized cat. In *Seventeenth Annual Computational Neuroscience Meeting: CNS*2008* Portland, OR, USA. 1924 July 2008 BMC Neuroscience 2008, 9 (Suppl 1):P125 doi:10.1186/1471-2202-9-S1-P125.